THE STUDY OF QUANTUM CUTTING IN YPO_4 AND YBO_3

by

YI ZHOU

(Under the Direction of Richard S. Meltzer)

ABSTRACT

Large bandgap materials doped with rare earth ions are currently of great interest as new vacuum UV phosphors for lighting and displays. In this thesis, the optical properties of YPO_4 and YBO_3 doped with Pr, Tm, Er, and Eu are described. The emission resulting from the VUV excitation of the parity allowed $4f^{n-1}5d^1$ states and their quantum efficiencies are studied. Relaxation between the $4f^{n-1}5d^1$ and nearby $4f^n$ excited states is observed for some of these ions and the dynamics of these excited states is studied. In doubly-doped samples, the prospects for quantum cutting using cross relaxation energy transfer in which some of the energy of the initially excited $4f^{n-1}5d^1$ state is transferred to an acceptor ion so that both donor and acceptor ions are left in an excited state from which they each can emit a photon are examined.

INDEX WORDS: Emission, Excitation, Quantum cutting, Cross relaxation

THE STUDY OF QUANTUM CUTTING IN YPO_4 AND YBO_3

by

YI ZHOU

B. Eng., Jinan University, P. R. CHINA 1991

A Thesis Submitted to the Graduate Faculty of The University of Georgia in Partial Fulfillment of the Requirements for the Degree

MASTER OF SCIENCE

ATHENS, GEORGIA

2005

THE STUDY OF QUANTUM CUTTING IN YPO_4 AND YBO_3

by

YI ZHOU

Major Professor: Richard S. Meltzer

Committee: William Denis
Yiping Zhao

Electronic Version Approved:

Maureen Grasso
Dean of the Graduate School
The University of Georgia
May 2005

ACKNOWLEDGEMENTS

I would like to thank Prof. Richard S. Meltzer, my major professor for his patience and advice in directing and implementing the research leading to this thesis. My thanks also to Dr. W. Jia for his many helpful discussions and his assistance with the experiment.

Finally, a special thanks to my wife and my parents for their support and encouragement without which this thesis may not have been possible.

TABLE OF CONTENTS

Page

CHAPTER 1

INTRODUCTION

In recent years, a growing interest has arisen in the luminescence spectroscopy of rare earths in the vacuum ultraviolet spectral region (VUV; $E \geq 50000$ cm^{-1}, $\lambda \leq 200$ nm). This is due to the need for new VUV phosphors for mercury-free fluorescent tubes and plasma display panels [1]. The phosphors used in mercury fluorescent tubes convert the ultraviolet (UV) emission of mercury discharge plasma into visible (white) light. Typical fluorescent lamp discharge emits UV radiation predominately at 254 nm, but also emit radiation at 185 nm (depending upon conditions, 10-20% of the UV radiation is emitted at 185 nm). The discharge conversion efficiency of electric power to 254 nm UV line is high (65%). The phosphor is responsible for nearly all the visible light produced by the lamp with the visible mercury lines contributing only a few percent to the total lamp light output. The phosphors have been optimized for efficient operation under excitation by 254 nm UV light [2]. Therefore, to make a noble gas discharge fluorescent tube competitive, quantum efficiencies higher than 100% are required, i.e. more than one visible photon should be obtained per absorbed VUV photon [3]. These VUV-excited materials are called “quantum cutting” or “multiphoton” phosphors.

The goal of our study is to find such multiphoton phosphors for VUV excitation. A successful phosphor will offer the prospect for great benefits to society by providing the scientific basis for realization of a new, highly efficient and environmentally benign lighting

technology. Lamps having improved efficiency would decrease the energy consumption for lighting thereby reducing the costs of lighting and the consumption of fossil fuels that contribute to environmental problems. In addition, the replacement of Hg in a standard fluorescent lamp by a rare-gas (VUV) excitation source would eliminate concerns regarding the disposal of Hg-based lamps.

The layout of this thesis is as follows: In Chapter 2, we will introduce the theory of quantum cutting and energy transfer. In Chapter 3 we will describe the equipments of experiment and the process of measurement. We will analyze the data and discuss the results in Chapter 4.

CHAPER 2

BACKGROUND AND THEORY

2.1 Introduction

In this chapter, we introduce the concepts of quantum cutting and downconversion. We also illustrate the two-step energy transfer from the ^6G_J level of Gd^{3+} to Eu^{3+}, the Er^{3+}–Gd^{3+}–Tb^{3+} downconversion system and the cross relaxation energy transfer for the ion-pair of Pr^{3+} and Tm^{3+}. The last ion pair will be examined in this thesis.

2.2 Quantum cutting

In 1957 Dexter mentioned the idea that an ultraviolet photon contains enough energy to be split into two visible photons [4]. Therefore it is in theory possible to obtain visible quantum efficiencies higher than 100% for VUV phosphors. In other words, after absorbing a VUV photon, the phosphor can produce two visible photons. This phenomenon is called quantum cutting (or two-photon luminescence, photon-cascade emission). For example, the phosphor YF_3: Pr^{3+} yields a room temperature quantum efficiency of 1.40 ± 0.15 under excitation by 185 nm radiation [5]. The process of quantum cutting in Pr^{3+} activated phosphors called cascade emission is shown in Fig. 2. 1. Incident VUV photons are absorbed via an allowed Pr^{3+} $4f \rightarrow 5d$ optical transition. The excitation decays nonradiatively to the $^1S_0$ level which decays radiatively to the $^1I_6$ level resulting in the generation of the first photon. A second transition that connects the ^3P levels with several of the ground state levels yields the second photon [2]. Unfortunately, the

photons emitted in the first step due to the $^1S_0 \rightarrow {}^1I_6$ transition have a wavelength of about 407 nm, for which the human eye is insensitive. So this cascade quantum cutting phosphor is not suitable for lighting applications.

2. 3 Energy transfer

2. 3. 1 Förster-Dexter energy transfer theory

A direct-energy-transfer theory was worked out by Förster for singlet-singlet transfer and by Dexter for triplet-triplet transfer for more than 50 years ago. It predicts the following:

(a) The excitation is transferred from a donor ion, D, to an acceptor ion, A, which are separated by a distance *R*, by a nonradiative process which is analogous to a simultaneous emission process on D and an absorption process on A. The interactions which cause energy transfer are electrostatic coupling, magnetic coupling, and/or exchange coupling between ions.

(b) The rate of dipole-induced transfer decreases as R^{-6} whereas the rate of exchange-induced transfer decreases as exp(-*2R/L*), where *R* is the donor-acceptor separation.

(c) The energy transfer rate is proportional to spectral overlap. Overlap of the corresponding emission and absorption bandwidths is necessary for conservation of energy [6].

2. 3. 2 Cross relaxation

The cross relaxation process is one in which the energy of excitation, initially localized on one ion, is partially transferred to a neighboring ion, leaving both ions in lower energy levels that decay rapidly to their respective ground states [7].

The cross relaxation rate for the case of dipole-dipole energy transfer can be estimated based on the Förster-Dexter dipole-dipole energy transfer theory. In Eq. 2. 1 the rate, P_{AB}^{dd} is

expressed in terms of f_A and f_B, the oscillator strengths of the two transitions labeled by A in Fig. 2. 4, the transition energies, ΔE, of each ion (in eV), the distance R between the two ions (in Angstroms), and the spectral overlap, S, (in cm^{-1}) of the downward and upward transitions [8].

$$P_{AB} = 1.4 \times 10^{24} f_A f_B S \Delta E^{-2} R^{-6} \qquad (2.1)$$

If we assume oscillator strengths of 10^{-2} and 10^{-6} for the $5d \rightarrow 4f$ and $4f \rightarrow 4f$ transitions, respectively, ΔE = 3 eV, and $S = 10^{-3}$, reflecting the fact that the $5d \rightarrow 4f$ downward transition is broad (about 1000 cm^{-1}), then we find for nearest neighbors at a distance of 3.5 Å, a rate of ~10^9 s^{-1} which is ten times greater than the radiative rate of ~10^8 s^{-1}. At more typical phosphor dopant concentrations of 2-5%, the energy transfer rate would be expected to be 10^7-10^8 s^{-1}, still competitive with the radiative rate. Exchange mediated energy transfer can be even much faster, but it will only be important for nearest neighbor distances.

Recently, an effort in quantum cutting phosphors centered on the couple Gd^{3+}-Eu^{3+} has been described in the literature. Two-step energy transfer from the ^6G_J level of Gd^{3+} to Eu^{3+} is possible, as is shown in Fig. 2.2. Incident VUV photons are absorbed via the Gd^{3+} $^8S_{7/2} \rightarrow {}^6G_J$ optical transition. In the first step (labeled as A in the figure) a cross-relaxation process transfers energy between Gd^{3+} in the ^6G_J state and Eu^{3+} in the ^7F_J ground state, resulting in Eu^{3+} in the $^5D_0$ excited state and Gd^{3+} in the ^6P_J state. This occurs with high probability because there is a good spectral overlap between the $^6G_J \rightarrow {}^6P_J$ transitions on Gd^{3+} and the $^7F_J \rightarrow {}^5D_0$ transitions on Eu^{3+} [9]. In the second step the Gd^{3+} ion in the ^6P_J state transfers the remaining excitation energy to a second Eu^{3+} ion, which is followed by fast relaxation to the ^5D_J states. Hence two photons may

be produced per incident VUV photon. Indeed, internal quantum efficiencies approaching nearly two in the $LiGdF_4:Eu^{3+}$ have been estimated.

However, the visible quantum cutting is not very efficient, because of the poor absorption of Gd^{3+} in the VUV. Using Er^{3+} and Tb^{3+} instead of the Eu^{3+} dopant in $LiGdF_4$ provides for efficient excitation and results in a quantum efficiency that is somewhat in excess of 100% [10]. In Fig. 2.3, the partial energy level scheme of the Er^{3+}–Gd^{3+}–Tb^{3+} downconversion system is given. Here, Er^{3+}–Gd^{3+} is the quantum cutting pair of ions. It can be calculated that several transitions from the $4f^{10}5d$ state of Er^{3+} to different ^4F_J and ^4G_J states overlap Gd^{3+} transitions from the ground state to respectively the ^6D_J, ^6I_J or ^6P_J states. Thus, upon excitation in the $4f^{10}5d$ levels of Er^{3+}, cross relaxation can take place between Er^{3+} and Gd^{3+}. After cross relaxation, Er^{3+} relaxes nonradiatively from the aforementioned ^4F and ^4G energy levels to the $^4S_{3/2}$ state, from which the emission of a green photon can occur. The excitation energy of Gd^{3+} migrates over the Gd^{3+} sublattice, until it reaches a Tb^{3+} (or Er^{3+}) ion. Then, energy transfer from Gd^{3+} can take place and a second visible photon is emitted after relaxation on the Tb^{3+} or Er^{3+} ions to their metastable states [11].

The energy transfer described above utilizes a cross relaxation scheme involving a parity allowed $4f^{11}5d \rightarrow 4f^{12}$ transition on Er^{3+} coupled with a transition within the $4f^7$ configuration of Gd^{3+} [10]. The demonstration of the latter scheme suggests that the use of parity allowed transitions on one of the ions in the ion-pair should be considered further and this provides motivation for the present work.

For cross relaxation energy transfer to be successful at down converting the energy, its rate must be competitive with these radiative rates. Fortunately, the multipolar interaction responsible for the energy transfer scales with these radiative rates, making possible a competitive cross relaxation energy transfer rate.

The cross relaxation energy transfer scheme is indicated on the energy level diagram shown in Fig. 2. 4 for the ion-pair of Pr^{3+} and Tm^{3+} which is studied in this thesis. After excitation of Pr^{3+} into its 4f5d configuration, a cross relaxation can occur as shown by the dashed arrows, labeled A, on both the Pr^{3+} and Tm^{3+} energy level diagrams. Here the Pr^{3+} ion undergoes a downward transition from the 4f5d configuration to its $^1D_2$ excited state in the f^2 configuration while simultaneously a Tm^{3+} ion undergoes an upward transition from its ground state to its $^1D_2$ level, conserving energy and leaving both ions in excited states from which each can emit a photon. In process B, the Pr^{3+} ion undergoes a downward transition from the 4f5d configuration to its $^3F_2$ excited state in the f^2 configuration while simultaneously a Tm^{3+} ion undergoes an upward transition from it ground state to its $^3P_2$ level, conserving energy and leaving both ions in excited states from which each can emit a photon.

Because the hosts YPO_4 and YBO_3 have large band gaps that fall well into the VUV, we decided to test the potential utility of a scheme for converting the exciting VUV photon into two visible photons using cross relaxation energy transfer involving a parity allowed $4f^{n-1}5d \rightarrow 4f^n$ transition on one ion and a transition within the $4f^{n'}$ configuration of a second ion in these materials.

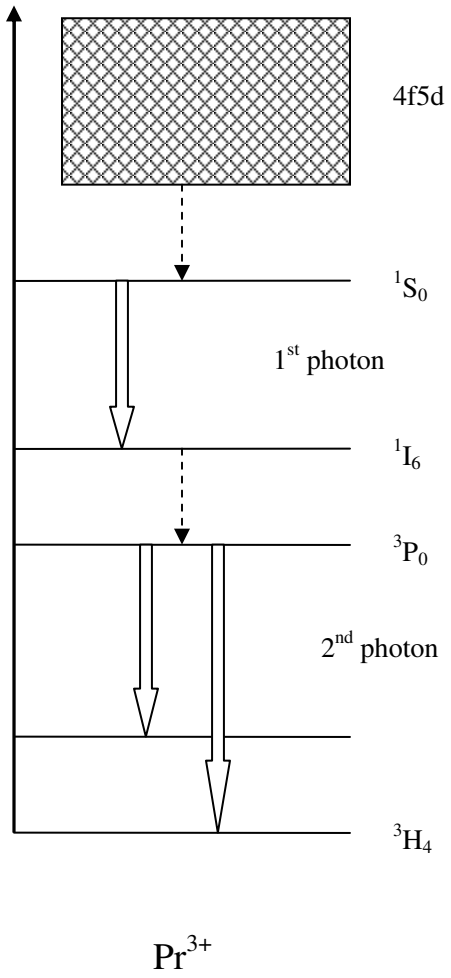

Fig. 2. 1. Schematic representation of multiphoton emission

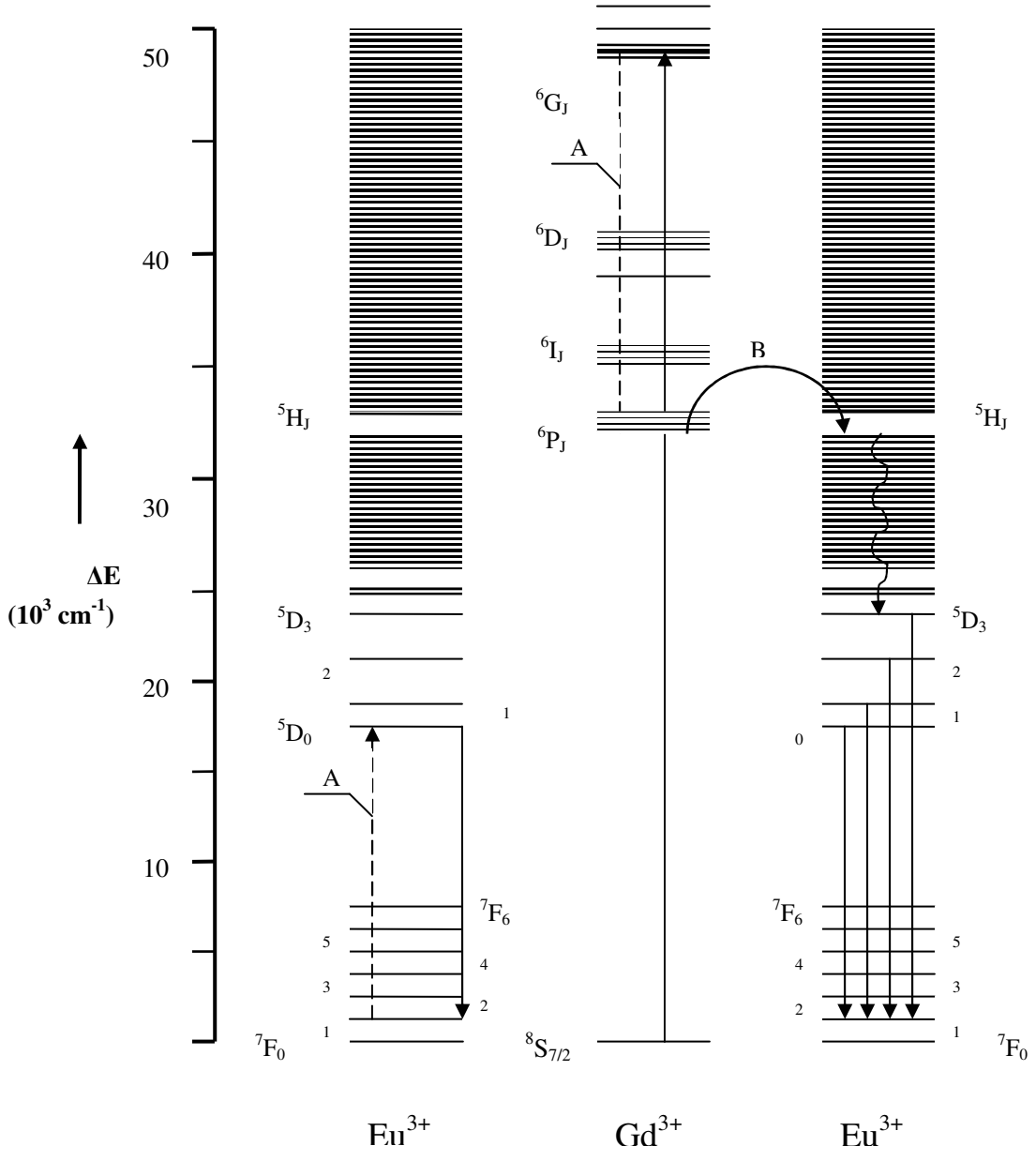

Fig. 2. 2. Energy level scheme of the Gd^{3+}- Eu^{3+} system

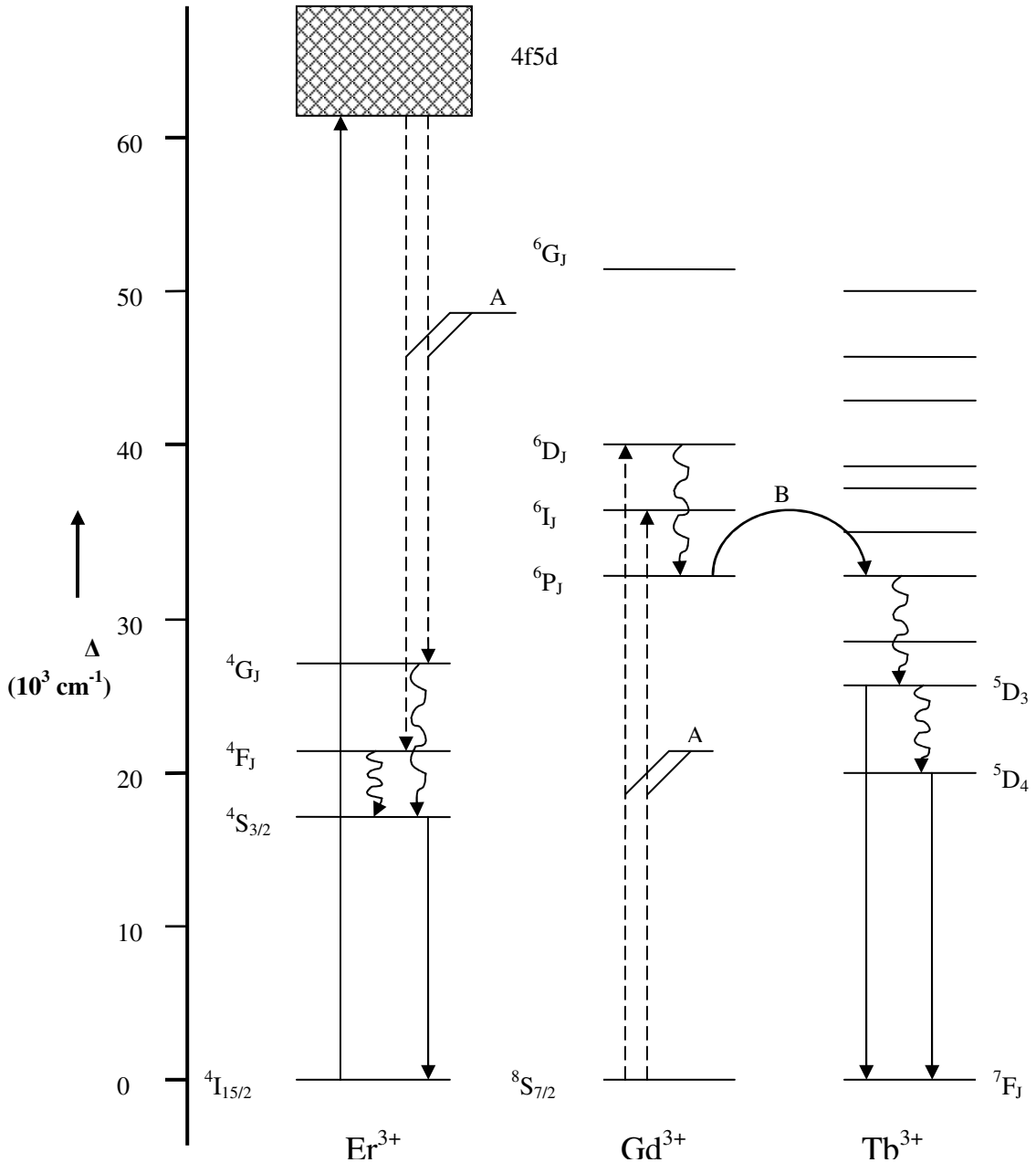

Fig. 2. 3. Energy level scheme of the Er^{3+}-Gd^{3+}- Tb^{3+}

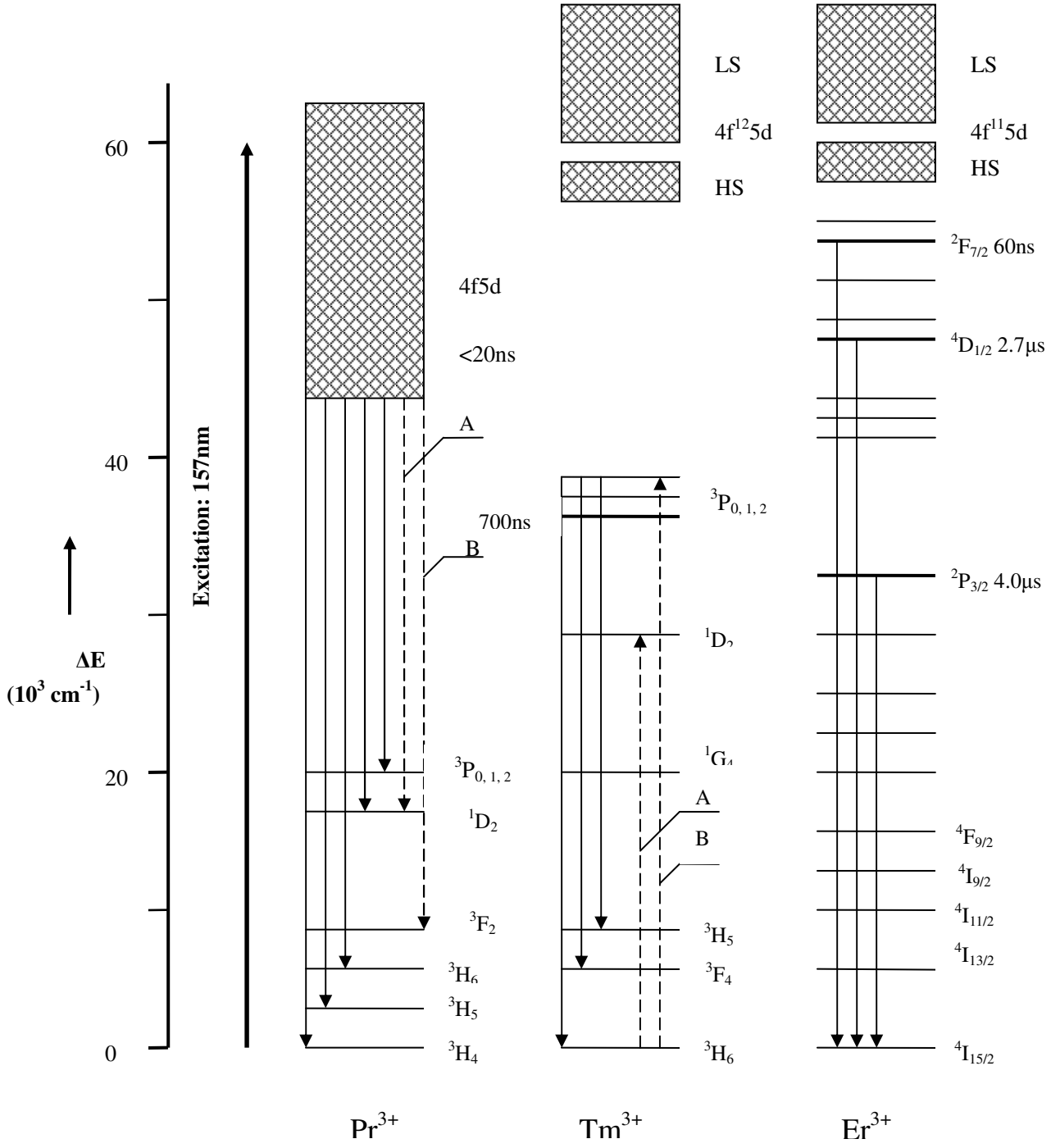

Fig. 2. 4 Energy level scheme for Pr^{3+}, Tm^{3+} and Er^{3+}

CHAPTER 3

EXPERIMENT

3.1 Introduction

In order to begin the investigation of quantum cutting in samples of YPO_4 and YBO_3 doped with trivalent rare earth ions, we first made a measurement of the emission spectra. Emission spectra were recorded with a CCD detector attached at the focal plane of a spectrometer. Emission was excited with monochromatic light from either a deuterium lamp filtered through a monochromator or the output of a F_2 gas discharge excimer laser emitting at 157 nm. Excitation spectra were performed with a deuterium lamp source and VUV monochromator to select and scan the excitation wavelength. The emission was detected with a photomultiplier tube (PMT) and either glass or interference filters to select the emission. The excitation spectra are measured relative to that of sodium salicylate whose absolute quantum efficiency is estimated as nearly constant at 55-60% over the excitation wavelength range of interest [12]. Time resolved emission spectra were obtained with the F_2 laser which had a temporal pulse width of 10ns. All emission and absorption spectra (except as noted) were fully corrected for the wavelength dependent response of the CCD or PMT as described below.

3. 2 Experimental Equipment

The setup which performs these measurements consists of an Acton Research Corporation VM502 VUV monochromator, equipped with a deuterium lamp, GAM Laser Inc.

EX5 Excimer Laser, a vacuum system, a Keithley 485 auto ranging pico ammeter, an Acton Research Corporation SpectraPro-150 spectrograph equipped with ST-6B CCD camera from Santa Barbara Instrument Group, two photomultiplier tubes described below and a TDS 460A Digitizing oscilloscope from Tektronix. The setup is shown in Fig. 3. 1.

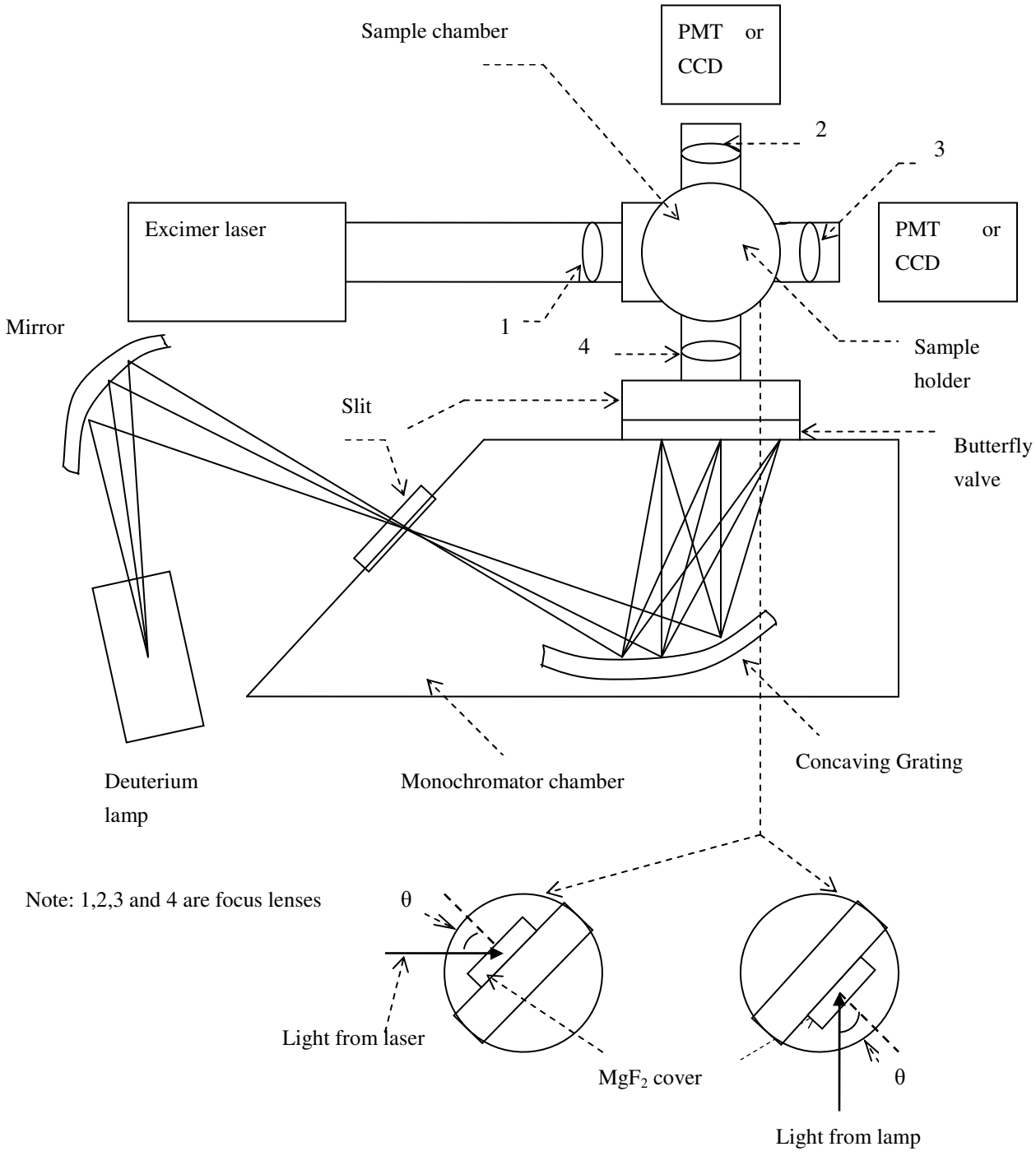

Fig. 3.1. Schematic setup for measurement

3. 2. 1 Light source and Monochromator

Two light sources were used in the experiment, a deuterium lamp and a F_2 gas discharge excimer laser emitting at 157 nm. This deuterium lamp provided a continuous emission spectrum from 115 nm to 370 nm.

First the light from the lamp strikes a mirror which focuses the reflected light onto the entrance slit of the VM 502 monochromator. This monochromator was used to select a narrow band of wavelengths for excitation of the sample from the continuous spectral output of the lamp. It is evacuated and contains a concave diffraction grating to disperse the light on to the exit slit.

The laser is air cooled. F_2 operation in the VUV is standard with up to 50 mW at 157 nm average output power at a repetition rate of 50 Hz. A new broadband optics set allows operation at 157 nm and 193 nm by simply changing the gas. The laser includes an internal vacuum pump and halogen filter; there is no requirement for an external vacuum system.

3. 2. 2 Vacuum System

The vacuum system is composed of two pumps, two pumping lines and two valves. One pump is a mechanical pump which initially pumps down the system; the other is a turbo-pump. One line connects the pump to the sample chamber; the other connects the pump to the monochromator chamber. The exit slit of the monochromator has a butterfly valve which can be closed to maintain the monochromator and lamp/mirror system under vacuum at all times.

3. 2. 3 Samples

Powder samples of YPO_4 and YBO_3 doped with trivalent rare earth ions were prepared by solid state reaction by Professor Douge Keszler and his group at Oregon State University. X-ray diffraction was used to make confirmation of a single phase of the correct crystal structure.

3. 3 Experiment

3. 3. 1 Measurement of emission spectra

Samples were loaded into the cells of the sample holder. These cells were 0.5 mm deep circular holes of 8 mm diameter which were covered with MgF_2 crystal windows. To reduce the interference from the MgF_2 covers, smaller or larger incident angles other than 45° of the VUV beam to the sample surface can be used. In this way, the reflected VUV beam from the MgF_2 covers does not directly hit the optics which can reflect the VUV excitation. In this series of experiments, we set θ at 35^o (see Fig. 3. 1). When the deuterium lamp was used as a light source, we recorded the spectra from the window with lens 3. When we used the laser to excite the samples, the sample holder was rotated by 180^o and we detected the spectra from the window with lens 2. The detection procedure is described in Appendix A.

The detector used in the experiment is an Acton Research Corporation SpectraPro-150 spectrograph equipped with ST-6B CCD camera from Santa Barbara Instrument Group. This spectrograph separates the emission light from the sample by wavelength and produces a spectrum from the sample. The emission spectrum is recorded by the CCD camera.

1. Wavelength calibration of the CCD

The wavelength calibration was done using emission lines, 253.65, 365.02, 435.84, 546.07, and 734.64 nm of a mercury lamp. The wavelengths determined from the manufacturer

calibration were off to these wavelengths by 1.027, 1.00, 0.985, 0.951, 0.908nm, respectively. So on average, the wavelength detected is 1nm below the actual wavelength.

2. Spectral calibration of CCD scan coverage

The detector coverage of this CCD is 85 nm with the 600g/m grating. The wavelength range of the emission spectrum is from about 210-940 nm. We could not get the whole spectrum at one time. We therefore divided the spectrum into 9 parts and measured them respectively. They were fit together to construct the whole emission spectrum. The spectral dispersion of the instrument ($d\lambda/dl$) was found to be slightly wavelength dependent. It decreases with wavelength almost linearly. The dispersion can be fit by the following equation:

$$d\lambda / dl = R_i = 0.34648 - 0.0000831 \times (\lambda_{i0} - 220) \qquad (3.\ 1)$$

Here λ_{i0} is the central wavelength of each detector coverage and dl is the distance between pixels. So, if giving the wavelength (for example, the central wavelength to be defined for each detector coverage), the spectral position of each pixel near that wavelength can be calculated. The wavelength at each pixel for each detector coverage range can be calculated:

$$\lambda = \lambda_{i0} + R_i \times (I - 125), \quad I \text{ from 1 to 250} \qquad (3.\ 2)$$

The scan groups we used in the measurement are shown in Table 3. 1. To obtain the actual wavelength, the 1 nm correction is added to the wavelength defined above for the CCD.

3. Spectral response of the CCD

a. Spectral response

The diffraction efficiency of a grating and sensitivity of a CCD detector are both a function of wavelength. Therefore, the spectral response of a CCD system needs to be measured

in order to obtain a true spectrum. In general, the spectral response of a CCD can be determined by measuring the radiation spectrum of a calibrated lamp (tungsten lamp).

λ_{i0} (nm)	R_i	Range (nm)
260	0.3432	217.443-302.900
345	0.3361	303.324-387.013
428	0.3292	387.179-469.150
510	0.3224	470.022-550.300
590	0.3157	550.853-629.463
668	0.3093	629.647-706.663
745	0.3029	707.440-782.863
820	0.2966	783.222-857.075
894	0.2905	857.978-930.308

Table 3. 1

The FEL Standard Lamp is a lamp calibrated against another lamp calibrated at NIST with ±2% accuracy. We used a series of interference filter before the lamp to reduce problems with stray light into spectrometer and measured the spectra. Because the spectrum of this lamp and the transmission of these filters are known, we could use Eq. (3.3) to calculate the spectral response (relative quantum yield) of the CCD system.

$$R(\lambda) = \frac{S(\lambda)}{\lambda I(\lambda)} = \text{Relative quantum yield} \qquad (3.3)$$

$S(\lambda)$ is the measured counts as a function of λ and $I(\lambda)$ is the known lamp output in mW/m^{2}nm at 50 cm from the lamp.

b. Scattered light

In practice, the measured radiation spectrum is always mixed with stray light originating from light of the input lamp beam which is scattered inside of the spectrometer. The stray light becomes more serious for a small spectrograph and for a CCD detector. It is especially serious in the UV, where the UV output of a tungsten lamp is three orders of magnitude weaker than that of the visible light, where it can add to the light at the wavelength of each pixel and overwhelm the emission.

Some of the light from the calibrated sources which enters the monochromator gets scattered by optical surfaces in the monochromator and reaches the CCD along random path. In order to reduce the influence of this stray light, a series of interference filters were used especially selected to transmit only the range of that scan. However the filter does not have 100% transmission in the wavelength range covered by one CCD scan. The detected signal contains the scattered light from the source which can transmit through the filter. The actual spectrum of the lamp in the spectral range is obtained by dividing the measured signal at each λ by the transmission of the filter at that wavelength.

$$S(\lambda_0) = \frac{S_{meas}(\lambda_0)}{T_{filter}(\lambda_0)} \tag{3. 4}$$

The corrected emission spectrum of samples can be obtained if the spectral response of the CCD is known:

$$E_0(\lambda) = CE(\lambda)R(\lambda) \quad (3.5)$$

E(λ) is the emission recorded by the CCD. *C* is an arbitrary constant which will be cancelled in the calculation of relative quantum efficiency introduced below.

3. 3. 2 Measurement of excitation spectra

An excitation spectrum is a type of fluorescence spectrum that the fluorescence intensity is produced as a function of wavelengths of the incident light.

As shown in Fig. 3. 1, we used the deuterium lamp as source light in the experiment. The light from the lamp strikes a mirror which focuses the reflected light onto the entrance slit of the VM 502 monochromator. This monochromator was used to select a narrow band of wavelengths for excitation of the sample from the continuous spectral output of the lamp. The output of the monochromator was focused onto the sample. The emission was detected with a photomultiplier tube (PMT). The details of operation procedure are shown in Appendix B.

The excitation spectra are measured relative to that of sodium salicylate whose absolute quantum efficiency is estimated as nearly constant at 55-60% over the wavelength range of interest. Therefore the excitation spectrum of sodium salicylate has a similar profile to that of the deuterium lamp. The relative excitation efficiency curve of the sample can be similar to its absorption spectrum if its quantum efficiency were constant but this is generally not the case.

In this thesis, the relative excitation spectrum of a sample is defined as:

$$R(\lambda_{excit}) = \frac{I_{sample}(\lambda_{excit})}{P(\lambda_{sample})}\left[\frac{I_{ref}(\lambda_{excit})}{P(\lambda_{ref})}\right]^{-1} = \frac{I_{sample}(\lambda_{excit})}{I_{ref}(\lambda_{excit})}\frac{P(\lambda_{ref})}{P(\lambda_{sample})} \quad (3.\ 6)$$

where $I_{sample}(\lambda_{excit})$ and $I_{ref}(\lambda_{excit})$ are the emission intensities measured by the PMT. $P(\lambda_{ref})$ and $P(\lambda_{sample})$ are spectral response of the PMT. The calculation of the $P(\lambda)$ is shown in Appendix C.

In this thesis, the excitation spectrum of a sample is expressed as:

$$I(\lambda) = L(\lambda)A(\lambda)Q(\lambda) \quad (3.\ 7)$$

where $L(\lambda)$ is the intensity of the excitation light source nearby the sample, which depends on the lamp profile and the output of the monochromator, A and Q are the absorption and quantum efficiency of the sample.

In a practical measurement, the result can be complicated by many factors. These include (1) the effect of scattered and background radiation; (2) correcting for the presence of multiple emission wavelengths where the quantum efficiency of the PMT has different values and (3) the consequence of the emission spectrum changing as a function of excitation wavelength. How to minimize the effects of these factors are described in Appendix C.

3. 3. 3 Measurement of life time

As shown in Fig. 3. 1, we used the laser to excite the sample. The laser beam was focused by the lens of focal length 2 inches onto the sample. The emission from sample was detected by a Hamamatsu R943 PMT from the window with lens 2. A TDS 460A Digitizing oscilloscope from Tektronix was connected to the PMT to record the time resolved spectrum. The detail of procedure of measurement is shown in Appendix D.

In a RC circuit, the product of R and C is a constant τ. In our measuring circuit, the capacitance is fixed for the oscilloscope. So when we measured the life time in different time resolution, we selected different resistors corresponding to the required temporal resolution. Use of a larger resistor gains stronger signals at the temporal response.

CHAPTER 4

RESULTS AND DISCUSSION

4. 1 Introduction

In this chapter, we analyze the emission and excitation spectra of YPO_4 and YBO_3. These samples are single-doped or double-doped with the trivalent rare earth ions. First we analyze the singly doped samples to obtain the basic properties of each ion and then we look at the doubly doped samples for energy transfer and quantum splitting. We also analyze the time resolved spectra of YPO_4 doped with Er^{3+}.

4. 2 Emission and excitation spectra of single doped YPO_4

4. 2. 1 Pr^{3+}: YPO_4

We first examine the optical properties of the single doped samples. The Fig. 4.1 shows the emission spectra for 1%, 5% and 10% Pr^{3+} doped YPO_4 at room temperature. All of these three samples were excited at 160 nm by the deuterium lamp. We can see the 4f5d emission in the region between 220 and 290 nm quenches with concentration. The large gap between the 4f5d state and the ^3P levels of Pr^{3+} results in dominant 4f5d emission. After expanding the spectra between 350 and 780 nm by a factor of 20, we also find a small amount of cascade emission from $4f^2$ ($^3P_0$ and $^1D_2$). The $^3P_0$ emission increases slightly with concentration.

The excitation spectra for 1%, 5% and 10% Pr^{3+} doped YPO_4 are shown in Fig. 4. 2. The range of detection wavelength is in the UV from 120 to 280 nm. We used a 280 nm long pass filter (WG280) to block the exciting light. In this figure we can see that the quantum efficiency is

very good for the 4f5d emission in samples with 1% and 5% Pr^{3+} doped YPO_4. The QE shows concentration quenching consistent with the emission results for 160 nm excitation.

4. 2. 2 Tm^{3+}: YPO_4

The excitation spectra for 0.2%, 1% and 10% Tm^{3+} doped YPO_4 are shown in Fig. 4.3. We used a WG320 filter to move the excitation light in measurement. The sharper feature at 160 nm is the $4f^{12}5d$ state and the broader feature at about 172 nm is the charge transfer (CT) band of Tm^{3+} which lies below the $4f^{12}5d$ state. In this figure, we find that the quantum efficiency is fairly high (about 25-30% absolute). In contrast to the case of Pr^{3+} the quantum yield is much less sensitive to concentration, dropping only by half at 10% Tm^{3+} concentrations. The quantum yield for 0.2% Tm^{3+} is a bit higher, about 30%, than for 1% Tm^{3+} and this may be an underestimate since the absorption has probably dropped significantly at only 0.2% Tm^{3+} levels.

The emission spectra for 0.2%, 1% and 10% Tm^{3+} doped YPO_4 are shown in Fig. 4. 4. We looked for the emission from the initially excited $4f^{12}5d$ configuration. However there is no evidence for emission from $4f^{12}5d$ despite the large gap between the lowest $4f^{12}5d$ state and the highest $4f^{13}$ levels. The charge transfer state (CT) probably plays a role in the relaxation the $4f^{12}5d$ state to $4f^{13}$ ($^3P_2$). It is perhaps the presence of this low-lying CT state that mediates the efficient relaxation to the $^3P_0$ emitting level. This occurs non-radiatively and does not yield quantum cutting. Most emission lines shown in these spectra are from $^3P_0$. We find that concentration quenching is not very strong for Tm.

4. 2. 3 Er^{3+}: YPO_4

The emission spectra of YPO_4 doped with Er (0.2%, 1% and 5%) are shown in Fig. 4. 5. We can see two groups of lines. One group are the emissions from $^2F_{7/2}$ to $^4I_{15/2}$, $^4I_{13/2}$, $^4I_{11/2}$, $^4I_{9/2}$, $^4F_{9/2}$, $^2H_{11/2}$ and $^2H_{9/2}$. The other are emissions from $^4D_{1/2}$ to $^4I_{13/2}$, $^4I_{11/2}$, $^4I_{9/2}$, $^4F_{9/2}$, $^4S_{3/2}$, $^2H_{11/2}$, $^2F_{7/2}$, $^2F_{5/2}$, $^2F_{3/2}$ and $^2H_{9/2}$. All emission arises from the $4f^{12}$ configuration. There is no emission from $4f^{10}5d$. This is to be expected for Er^{3+} since the $4f^{11}5d$ states lie just above the $4f^{12}$ levels so that multiphonon relaxation results in rapid relaxation to the metastable $^2F_{7/2}$ state (see Fig. 2. 4).

The excitation spectra of YPO_4 doped with Er (0.2%, 1% and 5%) are shown in Fig. 4. 6. A WG320 filter was used in the measurement to block the exciting light. The quantum yields relative to sodium salicylate of these 3 samples are less than 10% at room temperature. We can see a weak excitation at 170nm into the high spin (HS) 5d level which occurs for all rare earths with a f^n configuration which is more than half filled (n>7). It lies directly below the strongest excitation peak of the low spin state. The host absorption feature reported below 150 nm at T=10K [13] is not observed at room temperature. The observed quantum yield relative to sodium salicylate falls at lower Er^{3+} concentrations, probably due to decreased 5d absorption.

4. 3 Emission and excitation spectra of double doped YPO_4

4. 3. 1 Pr-Tm couple

We now turn to the issue of quantum cutting using cross relaxation energy transfer from the $4f^{n-1}5d$ configuration of the trivalent rare earth ions. As noted in Fig. 2. 4 by the dashed arrows labeled A and B, energy conserving cross relaxation schemes exist for the Pr^{3+}-Tm^{3+} pair. Process A is very attractive since it leaves both ions in visible emitting excited states. However, as seen for YPO_4 in Fig. 4. 1, emission from 4f5d to $^1D_2$ is much weaker than that to the ^3H_J and

^3F_J levels. Thus the oscillator strength of this transition is probably only about 10^{-4} reducing expected energy transfer rates below 10^6 s^{-1} (Eq. 2. 1 in Sec. 2. 3) which is insufficient to compete with the radiative rate. While process B would not leave Pr^{3+} in a visible emitting state, it can still provide a proof of concept demonstration.

The emission spectrum of YPO_4 double-doped with 1% Pr^{3+} and 5% Tm^{3+} is shown in Fig. 4. 7. We can see the emission of Pr^{3+} from 4f5d to $4f^2$ (^3H, ^3F). Strong Tm^{3+} absorptions to the ^3P_J levels occur in the range of 268-289 nm as indicated on the bottom of Fig. 4. 7; there is a good resonance for cross relaxation energy transfer from 4f5d of Pr^{3+} involving $^3P_2$ of Tm.

To test this idea we obtained the excitation spectrum of YPO_4 double-doped with 1%Pr, 5%Tm. Fig. 4. 8 shows no evidence of the Pr^{3+} absorption when only the Tm^{3+} emission is detected. This was done by using a 350 nm interference filter with 10 nm bandwidth before the PMT to detect Tm^{3+} emission from $^3P_0$. Only the Tm^{3+} excitation features of the CT and $4f^{12}5d$ states are observed. Therefore there is little energy transfer despite the favorable resonance conditions.

4. 3. 2 Pr-Er couple

Cross relaxation energy transfer for the Pr^{3+}-Er^{3+} couple has also been investigated in YPO_4. We would like to see the energy transfer from Pr to Er. From the emission spectrum of YPO_4 double-doped with 1% Pr and 10% Er shown in Fig. 4. 9, we can see that the strong 4f5d emission of Pr^{3+} between 230-270 nm overlaps a number of absorptions of Er^{3+} (see Fig. 4. 5). Unfortunately these Er^{3+} transitions are quite weak with small oscillator strengths. Indeed, excitation of a sample containing 1% Pr^{3+} and 10% Er^{3+} at 188 nm, where only Pr^{3+} absorbs (see

Fig. 4. 2), yields no observable Er^{3+} emission. This means that there is little Pr to Er energy transfer after excitation of the 4f5d state of Pr^{3+} at 188 nm.

4. 3. 3 Pr-Eu couple

For Eu^{3+} in YPO_4, the CT transition of Eu^{3+} overlaps strongly with the 4f5d absorption of Pr^{3+} so that it is difficult to identify cross relaxation energy transfer. There certainly is overlap between the 4f5d emission of Pr^{3+} and the large density of Eu^{3+} transitions within the $4f^6$ configuration. The emission spectrum of YPO_4 double-doped with 1% Pr and 5% Eu is shown in Fig. 4. 10. We can see the 4f5d emission of Pr^{3+} is strongly quenched in the presence of Eu^{3+}. This suggests that rapid energy transfer from Pr^{3+} to Eu^{3+} occurs and competes with the radiative decay of Pr^{3+}. However this is most likely to leave the Pr^{3+} ion in one of its low-lying levels from which visible emission will not occur. Indeed, very little visible emission from Pr^{3+} is seen in either of these samples.

The excitation spectrum of YPO_4 double-doped with 1% Pr and 5% Eu is shown in Fig. 4. 11. A WG280 filter was used in the measurement. It is compared with the excitation of single doped Pr^{3+} or Eu^{3+}. It does not reveal much about the Pr^{3+} to Eu^{3+} energy transfer because of the overlap of the CT band of Eu^{3+} with the 4f5d absorption of Pr^{3+}. However, at all excitation wavelengths, even the Eu^{3+} minimum at 160nm, the emission is almost totally from Eu^{3+} suggesting significant energy transfer. The absence of Pr^{3+} emission suggests that quantum splitting is not occurring although an energy transfer back to Eu^{3+} may quench the emission.

4. 4 Emission and excitation spectra of YBO_3

4. 4. 1 Pr^{3+}: YBO_3

The emission spectra of YBO_3 doped with 1% and 5% Pr are shown in Fig. 4. 12. We can see the 4f5d emission in the region between 220 and 290 nm and that the 4f5d emission quenches with concentration. Almost all the emission is in the UV from the 4f5d configuration. The spectrum, from 370 to 700 nm, expanded by a factor of 50, shows a small amount of cascade emission as evidenced from the $4f^2$ ($^1D_2$) emission. No $^3P_0$ emission is observed, consistent with previous results indicating the dominance of multiphonon relaxation to $^1D_2$ [7].

The excitation spectra of YBO_3 doped with 1% and 5% Pr are shown in Fig. 4. 13. A WG280 filter was used before the PMT. The sample containing 1% Pr^{3+} exhibits strong emission from the 4f5d state with a quantum yield relative to sodium salicylate of 1.2, implying an absolute quantum yield of about 0.6 for excitation between 230 to 250 nm. This exceeds the value for YPO_4: Pr^{3+} in Fig. 4. 2. Concentration quenching of the Pr^{3+} emission is indicated but it does not populate $^3P_0$ or $^1D_2$.

4. 4. 2 YBO_3 double doped with Pr^{3+} and Tm^{3+}

The emission spectrum of YBO_3 doped with 1% Pr and 5% Tm is shown in Fig. 4. 14. We can see a good resonance for cross relaxation energy transfer from 4f5d of Pr^{3+} involving $^3P_2$ of Tm. However the presence of Pr^{3+} 4f5d emission indicates that energy transfer is not complete if it occurs at all. Comparing Fig. 4. 14 with Fig. 4. 7, the emission spectrum of YPO_4 doped with 1% Pr and 5% Tm, we find that the 4f5d Pr^{3+} emission features are shifted by about 20nm to the red relative to those of YPO_4, as expected, since the 4f5d levels in YBO_3 are predicted to lie about 3100 cm^{-1} below the corresponding levels in YPO_4 [14].

We use two different filters to measure the excitation spectrum of YBO_3 double doped with 1% Pr and 5% Tm. One is a 450 nm interference filter which is used to monitor the Tm emission only. The other is a $NiSO_4$ filter which transmits from 250 nm to 340 nm and is used to monitor Pr. We put these two spectra and the excitation spectrum of YBO_3 single doped with 1% Pr together in Fig. 4. 15. The spectrum detecting only the Tm^{3+} emission shows little of any features of the Pr^{3+} excitation spectrum indicating the absence of energy transfer. The overlap of the 4f5d emission of Pr^{3+} with the absorption from $^3H_6$ to ^3P_J states of Tm^{3+} is even more favorable than in YPO_4 and yet virtually no emission from Tm^{3+} is observed when exciting the 4f5d levels of Pr^{3+}.

We also measured the emission spectrum of YBO_3 doped with 1% Pr and 5% Tm by exciting Pr at 238 nm. The emission spectrum shown in Fig. 4. 16 shows that there is no Tm^{3+} emission. It confirms the absence of Pr^{3+} to Tm^{3+} energy transfer.

4. 4. 3 YBO_3 double doped with Pr^{3+} and Eu^{3+}

For Eu^{3+} in YBO_3, the CT transition overlaps strongly with the 4f5fd absorption of Pr^{3+} so that it is difficult to identify cross relaxation energy transfer from Pr^{3+} to Eu^{3+}. There certainly is overlap between the 4f5d emission of Pr^{3+} and the large density of Eu^{3+} transitions within the $4f^6$ configuration. We excited YBO_3 doped with 1% Pr and 5% Eu at 160 nm. The spectrum is shown in Fig. 4. 17. We find the emission of Pr^{3+} is almost absent. This suggests that rapid energy transfer from Pr^{3+} to Eu^{3+} occurs and competes with the radiative decay of Pr^{3+}. This is most likely to leave the Pr^{3+} ion in one of its low-lying levels from which visible emission will not occur. Indeed, very little visible emission from Pr^{3+} is seen in either of these samples.

4. 5 Dynamics of Relaxation of YPO_4: Er

The emission spectra of YPO_4 doped with Er^{3+} shows three groups of lines from the three metastable levels indicated by the bold lines in the energy level diagram of Fig. 2. 4. We excited the sample of YPO_4 doped with Er at 157 nm with the F_2 laser and detected the emissions at 227 nm, 289 nm and 470 nm with a Hamamatsu R943 PMT.

The time resolved spectrum of the emission at 227 nm is shown in Fig. 4. 18. We used two functions to fit this curve and got two lines. The decay time of one line was short (0.06 μs) and the other was long (0.4 μs). For the time resolved spectrum of the emission at 470 nm, which was shown in Fig. 4. 19, we also used two functions to fit the curve. We got two lines that the decay time of one line was 0.42 μs and the other was 4.15 μs. We found that the decay time of the line with smaller slope in Fig. 4. 18 was almost the same as that of the line with larger slope in Fig. 4. 19. So we believe that these two lines are emissions from broadband background emission. We concluded therefore that the decay time of $^2F_{7/2}$ emission was 0.06 μs and the decay time of $^2P_{3/2}$ emission was 4.15 μs. The time resolved spectrum of the emission at 289 nm was shown in Fig. 4. 20. After fitting the curve, we found that the decay time of $^4D_{1/2}$ emission was 2.5 μs.

These time resolved spectra at 300K show that all three of the emitting levels appear immediately (<20ns) after excitation of the $4f^{11}5d$ state. This is contrary to the expected mulitphonon relaxation process that would populate the levels sequentially from higher to lower energy and implies some other non-radiative channel leading directly and rapidly from the $4f^{11}5d$ state to all three of these states of the $4f^{12}$ configuration.

4. 6 Conclusion

The quantum splitting of the high energy $4f^{n-1}5d$ electronic states of trivalent rare earth sensitizer ions into shared excitation of lower energy on this sensitizer and another activator ion using cross relaxation energy transfer does not seem promising in the hosts YPO_4 or YBO_3. Of the ions Pr^{3+}, Tm^{3+}, Er^{3+} and Eu^{3+}, only Pr^{3+} shows emission from its 5d state at room temperature. Attempts to observe cross relaxation energy transfer from Pr^{3+} to Tm^{3+} and Er^{3+} at 5% dopant levels were unsuccessful, despite the fact the energy conserving pathways exist. Thus, even using a parity allowed $5d \rightarrow 4f$ transition on one of the ions does not provide a sufficiently large dipole-dipole strength to compete with radiative decay of the 5d states. In order to obtain sufficient energy transfer, it will probably be necessary to invoke exchange interactions and energy migration which will occur only in stoichiometric samples as previously demonstrated for $LiGdF_4:Eu^{3+}$ [3]. For both Er^{3+} and Tm^{3+} in YPO_4, the 5d emission is quenched and emission from the $4f^n$ configuration appears immediately (<20 ns), implying a very fast relaxation from the lowest $4f^{n-1}5d$ state to the $4f^n$ states, even when the energy gap between the lowest $4f^{n-1}5d$ state and $4f^n$ states are much larger than can be bridged by multiphonon relaxation.

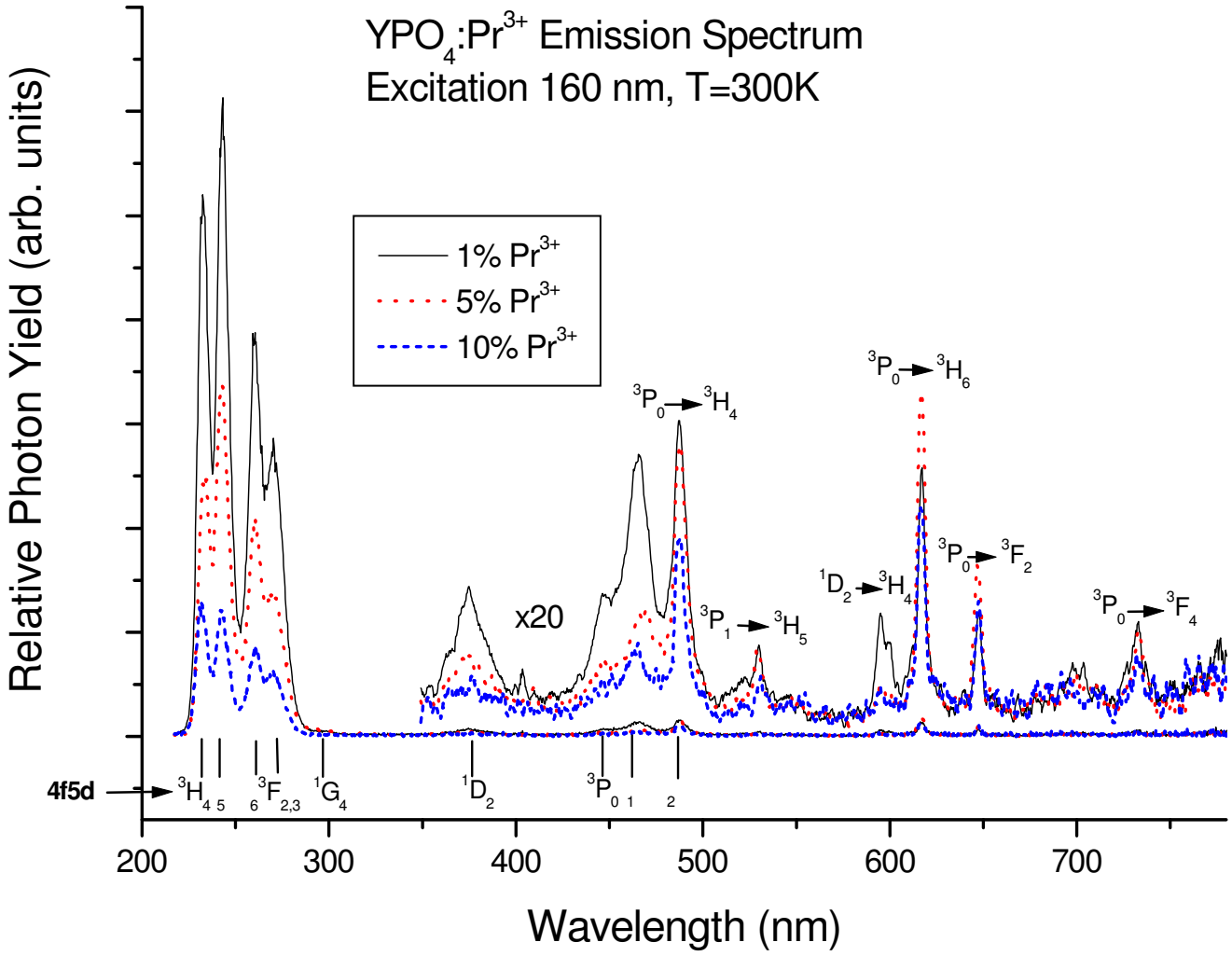
YPO4:Pr3+ Emission Spectrum
Excitation 160 nm, T=300K
1% Pr3+
5% Pr3+
10% Pr3+
Relative Photon Yield (arb. units)
Wavelength (nm)
200
300
400
500
600
700
x20
4f5d
3H4 5
3F2,3
6
1G4
1D2
3P0 1
2
3P0 → 3H4
3P1 → 3H5
3P0 → 3H6
1D2 → 3H4
3P0 → 3F2
3P0 → 3F4

Fig. 4. 1

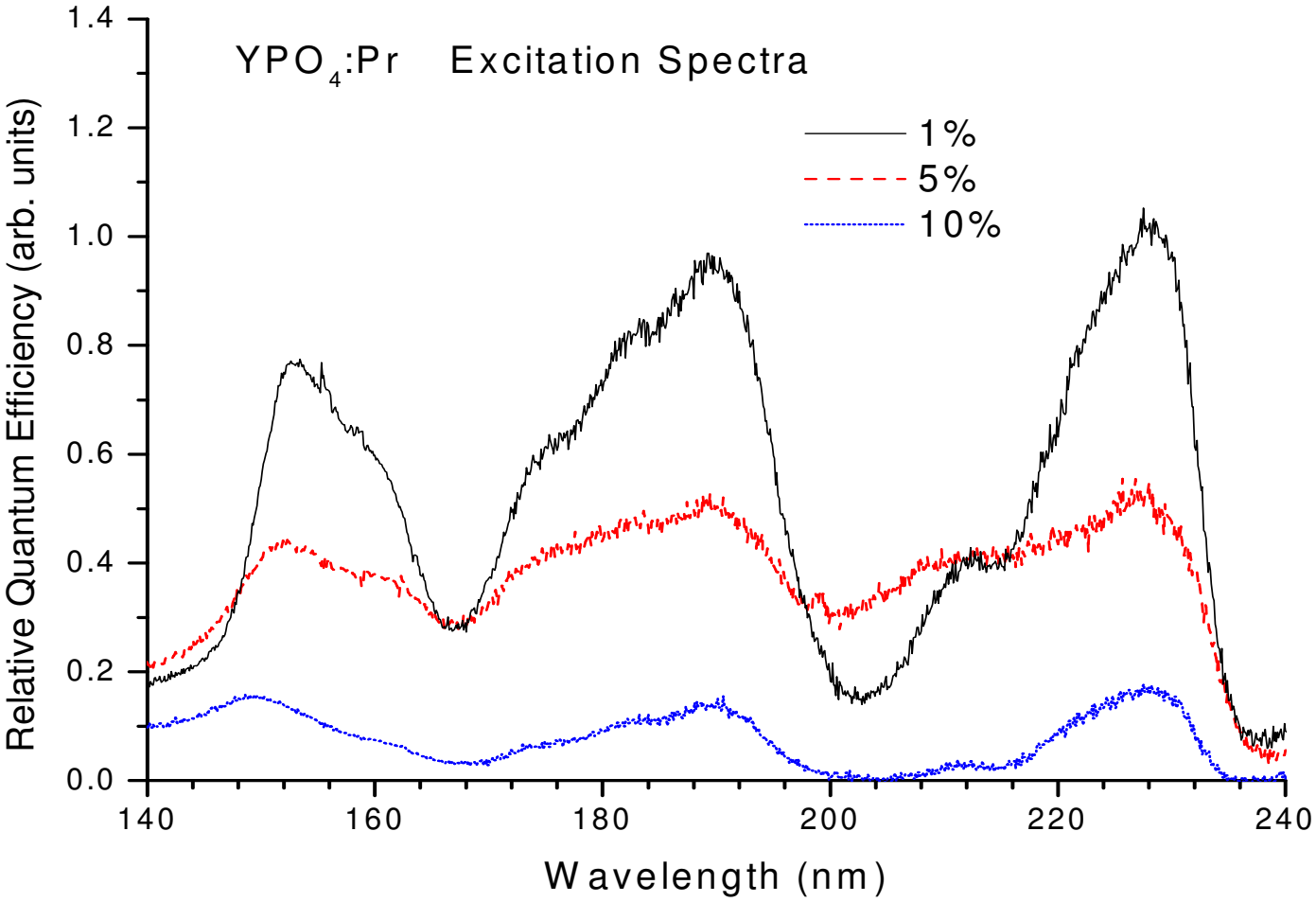
YPO4:Pr Excitation Spectra
1%
5%
10%
Relative Quantum Efficiency (arb. units)
Wavelength (nm)
0.0
0.2
0.4
0.6
0.8
1.0
1.2
1.4
140
160
180
200
220
240

Fig. 4. 2

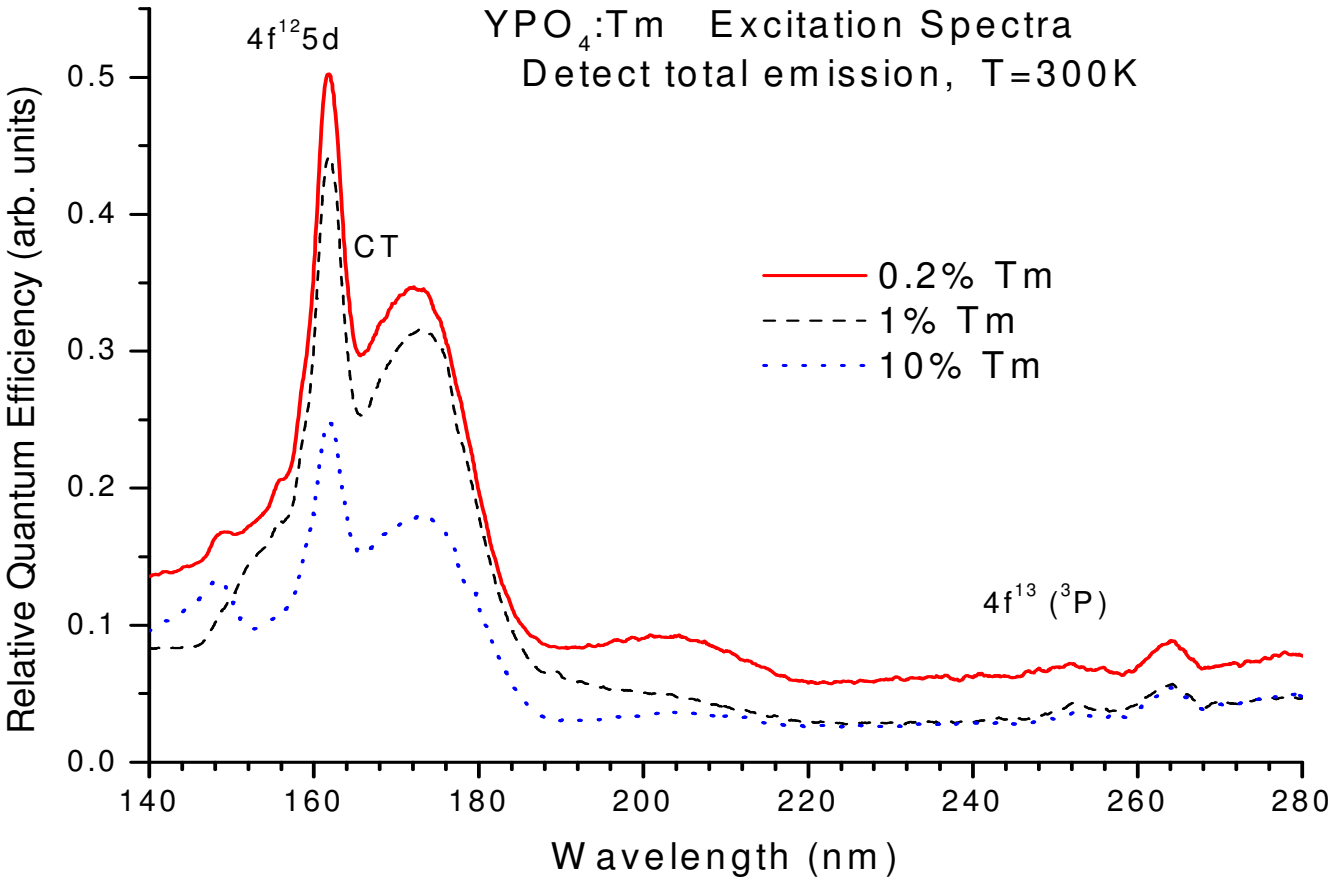
YPO4:Tm Excitation Spectra
Detect total emission, T=300K
4f12 5d
CT
4f13 (3P)
0.2% Tm
1% Tm
10% Tm
Relative Quantum Efficiency (arb. units)
Wavelength (nm)
0.0
0.1
0.2
0.3
0.4
0.5
140
160
180
200
220
240
260
280

Fig. 4. 3

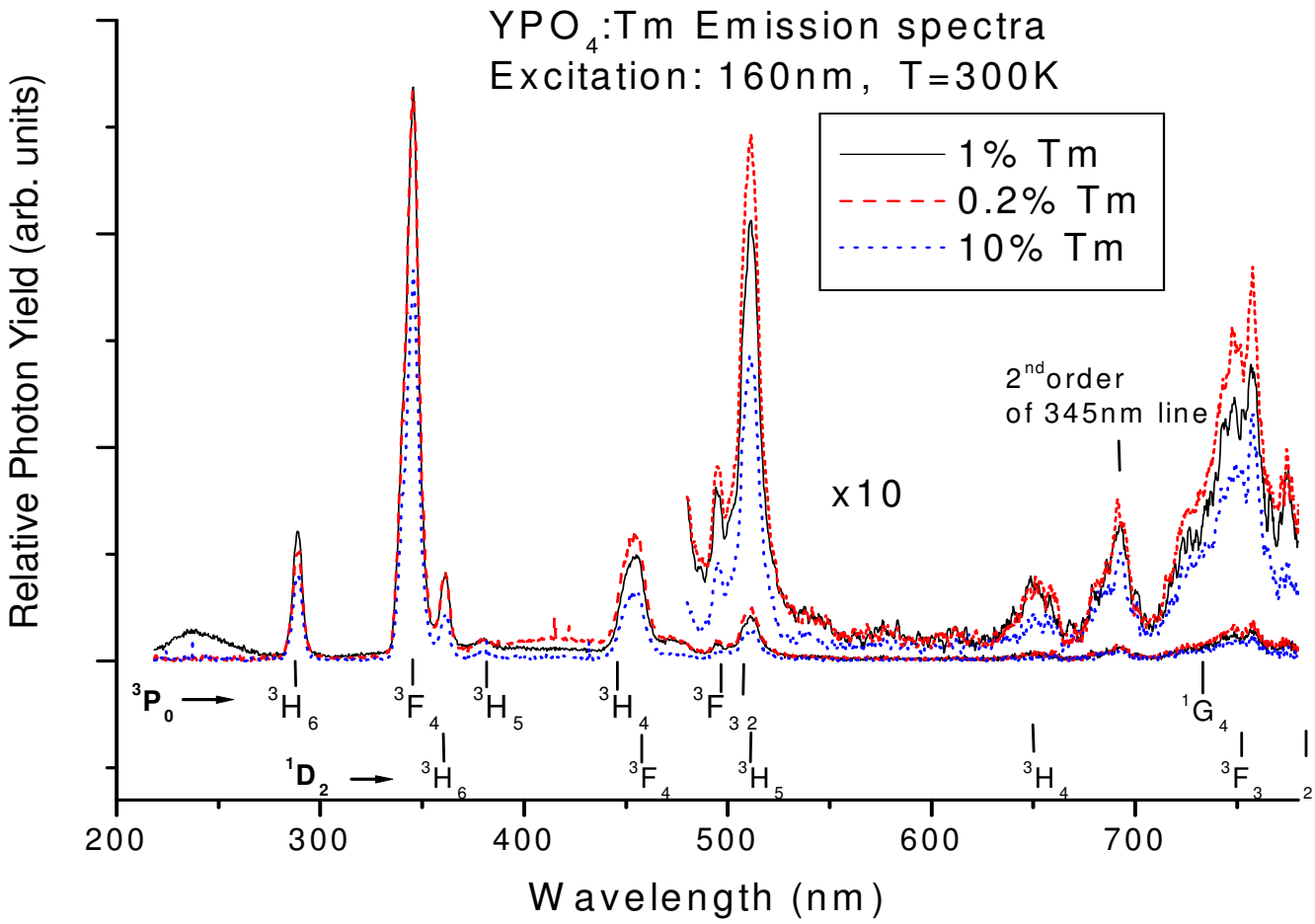
YPO4:Tm Emission spectra
Excitation: 160nm, T=300K
1% Tm
0.2% Tm
10% Tm
2nd order
of 345nm line
x10
Relative Photon Yield (arb. units)
Wavelength (nm)
200
300
400
500
600
700
3P0
3H6
3F4
3H5
3H4
3F3 2
1G4
1D2
3H6
3F4
3H5
3H4
3F3
2

Fig. 4. 4

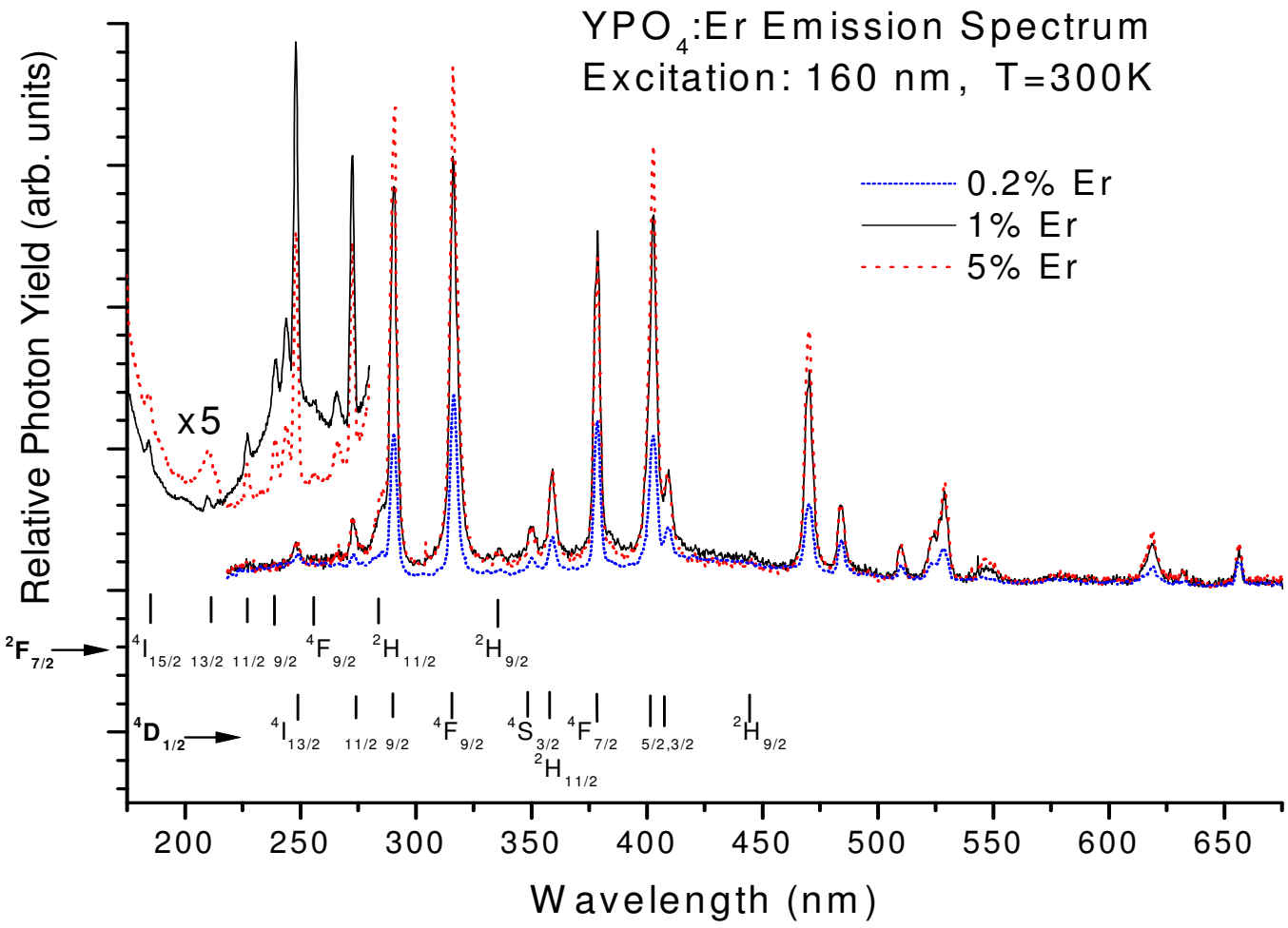
YPO4:Er Emission Spectrum
Excitation: 160 nm, T=300K
0.2% Er
1% Er
5% Er
x5
Relative Photon Yield (arb. units)
Wavelength (nm)
200
250
300
350
400
450
500
550
600
650
2F7/2
4I15/2 13/2 11/2 9/2
4F9/2
2H11/2
2H9/2
4D1/2
4I13/2 11/2 9/2
4F9/2
4S3/2
2H11/2
4F7/2
5/2,3/2
2H9/2

Fig. 4. 5

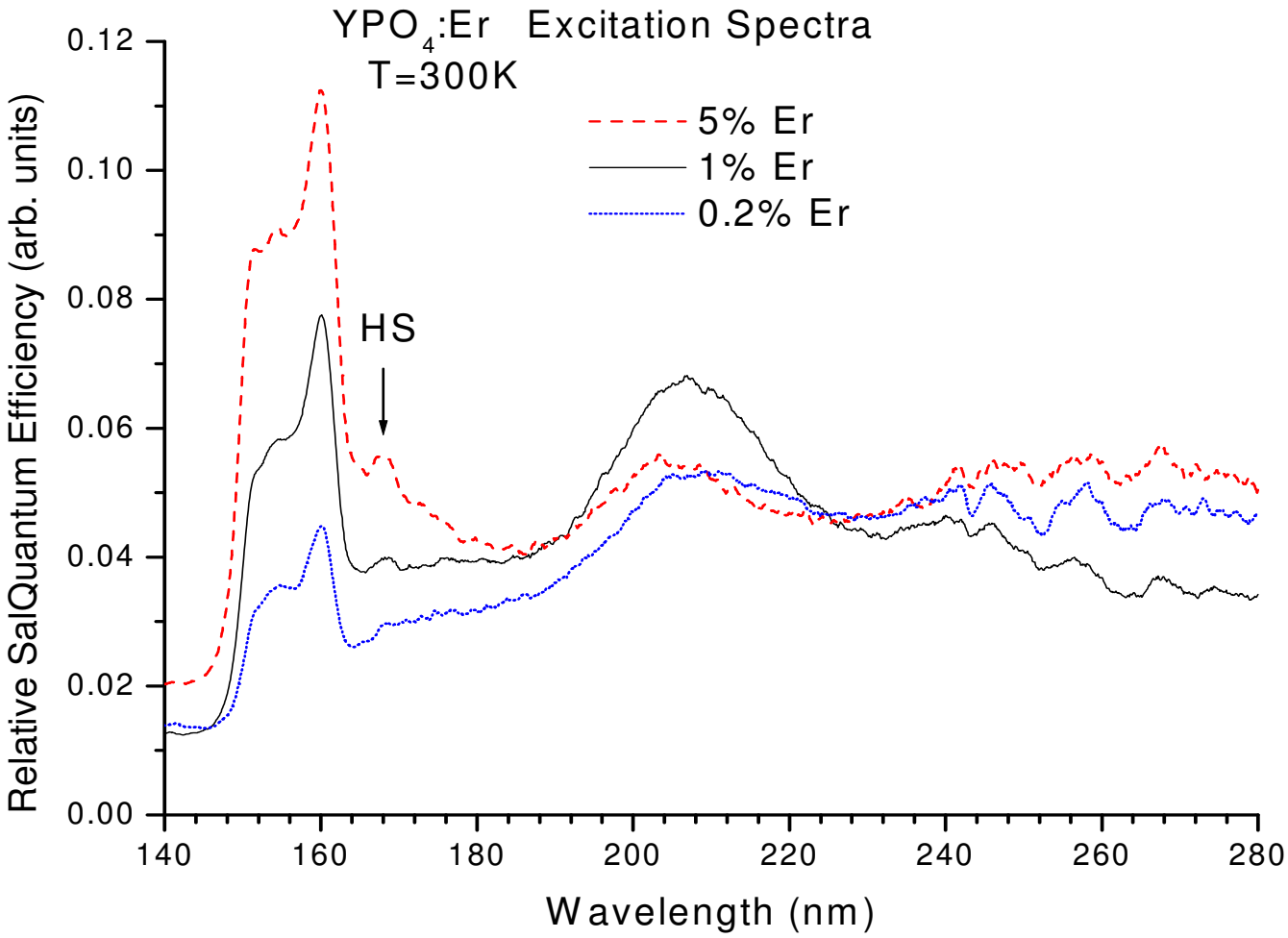
YPO4:Er Excitation Spectra
T=300K
5% Er
1% Er
0.2% Er
HS
Relative SalQuantum Efficiency (arb. units)
0.00
0.02
0.04
0.06
0.08
0.10
0.12
140
160
180
200
220
240
260
280
Wavelength (nm)

Fig. 4. 6

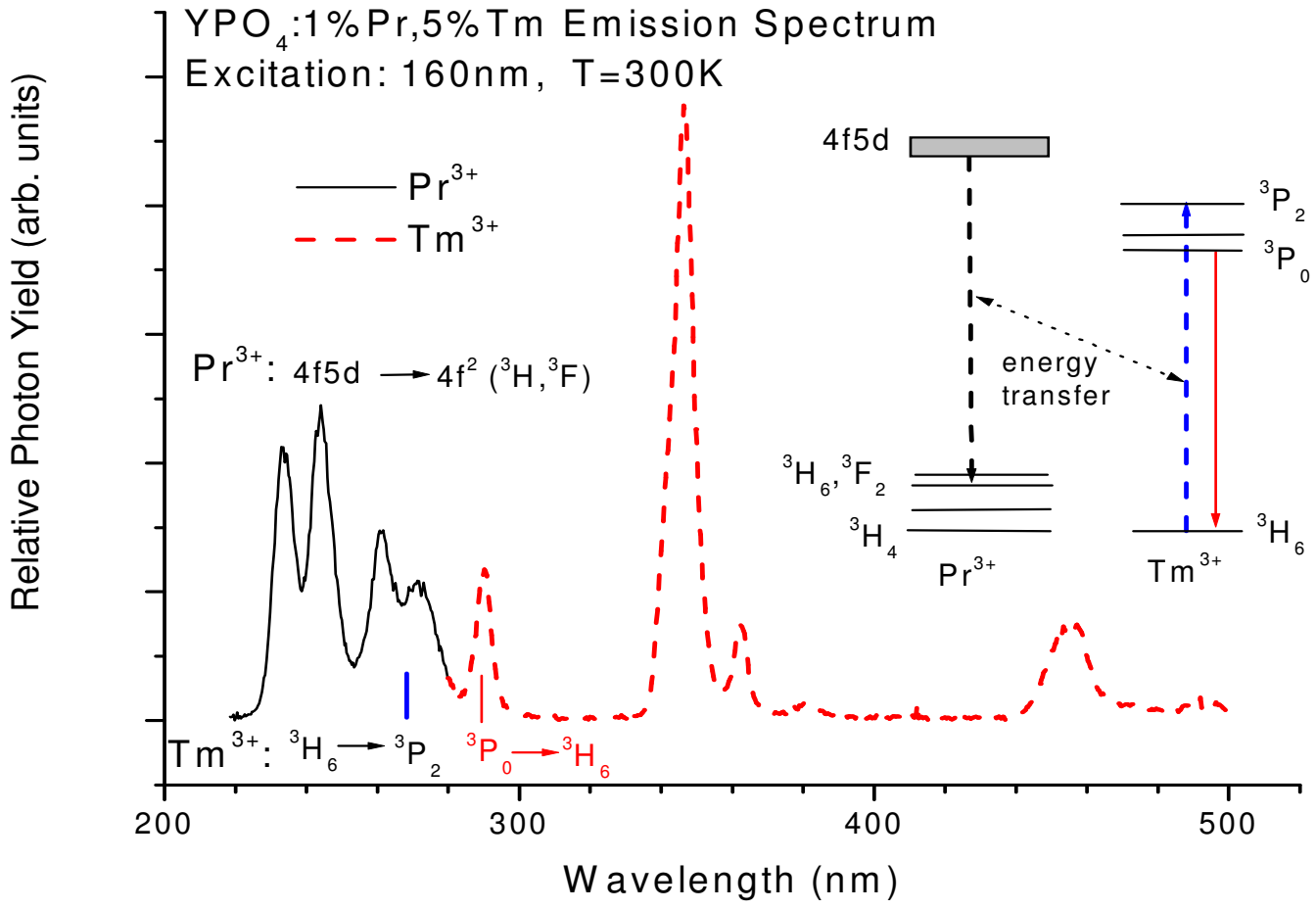
YPO4:1%Pr,5%Tm Emission Spectrum
Excitation: 160nm, T=300K
Relative Photon Yield (arb. units)
Wavelength (nm)
200
300
400
500
Pr3+
Tm3+
Pr3+: 4f5d → 4f2 (3H,3F)
Tm3+: 3H6 → 3P2
3P0 → 3H6
4f5d
energy transfer
3H6,3F2
3H4
Pr3+
3P2
3P0
3H6
Tm3+

Fig. 4. 7

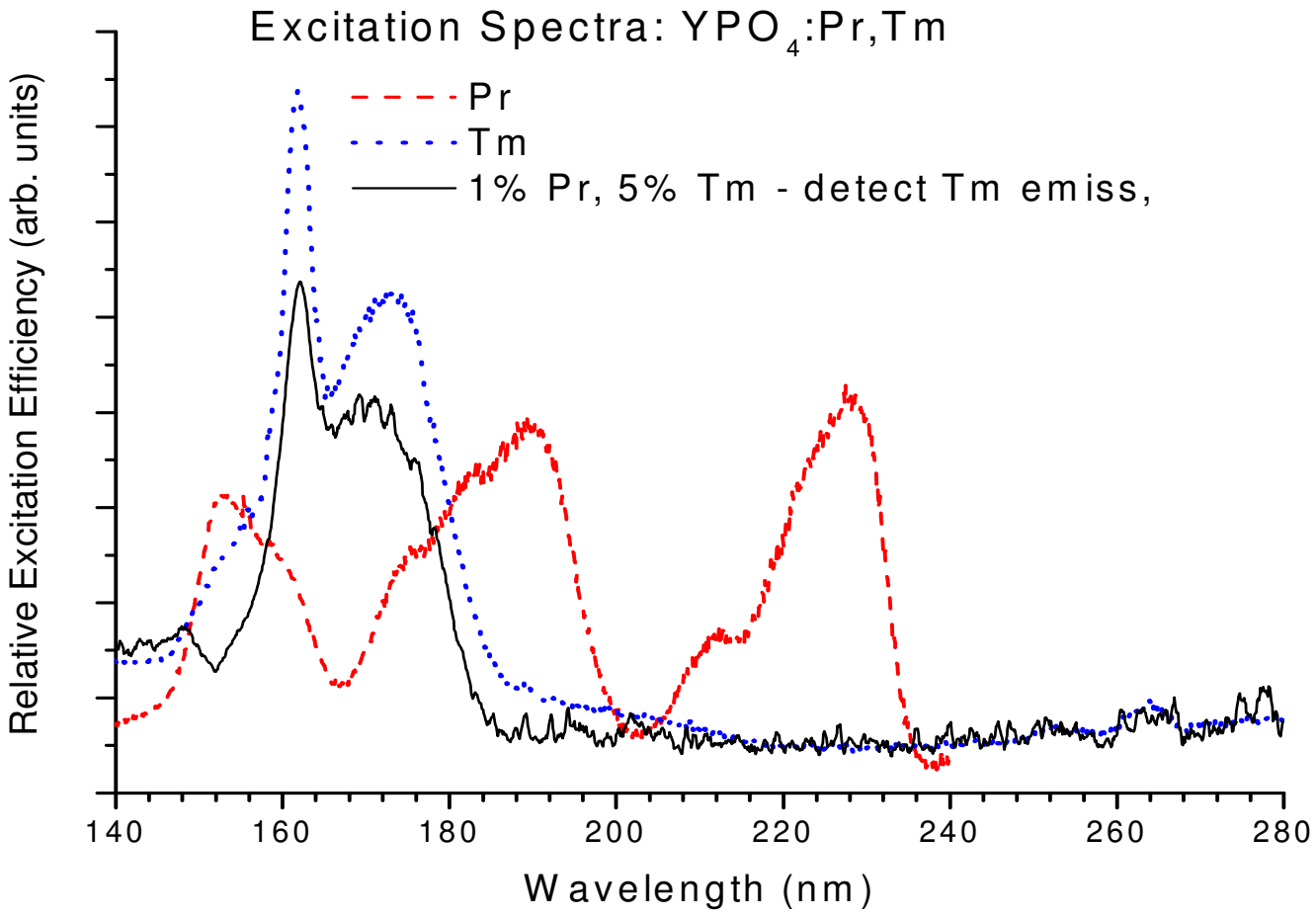
Excitation Spectra: YPO4:Pr,Tm
Pr
Tm
1% Pr, 5% Tm - detect Tm emiss,
Relative Excitation Efficiency (arb. units)
140
160
180
200
220
240
260
280
Wavelength (nm)

Fig. 4. 8

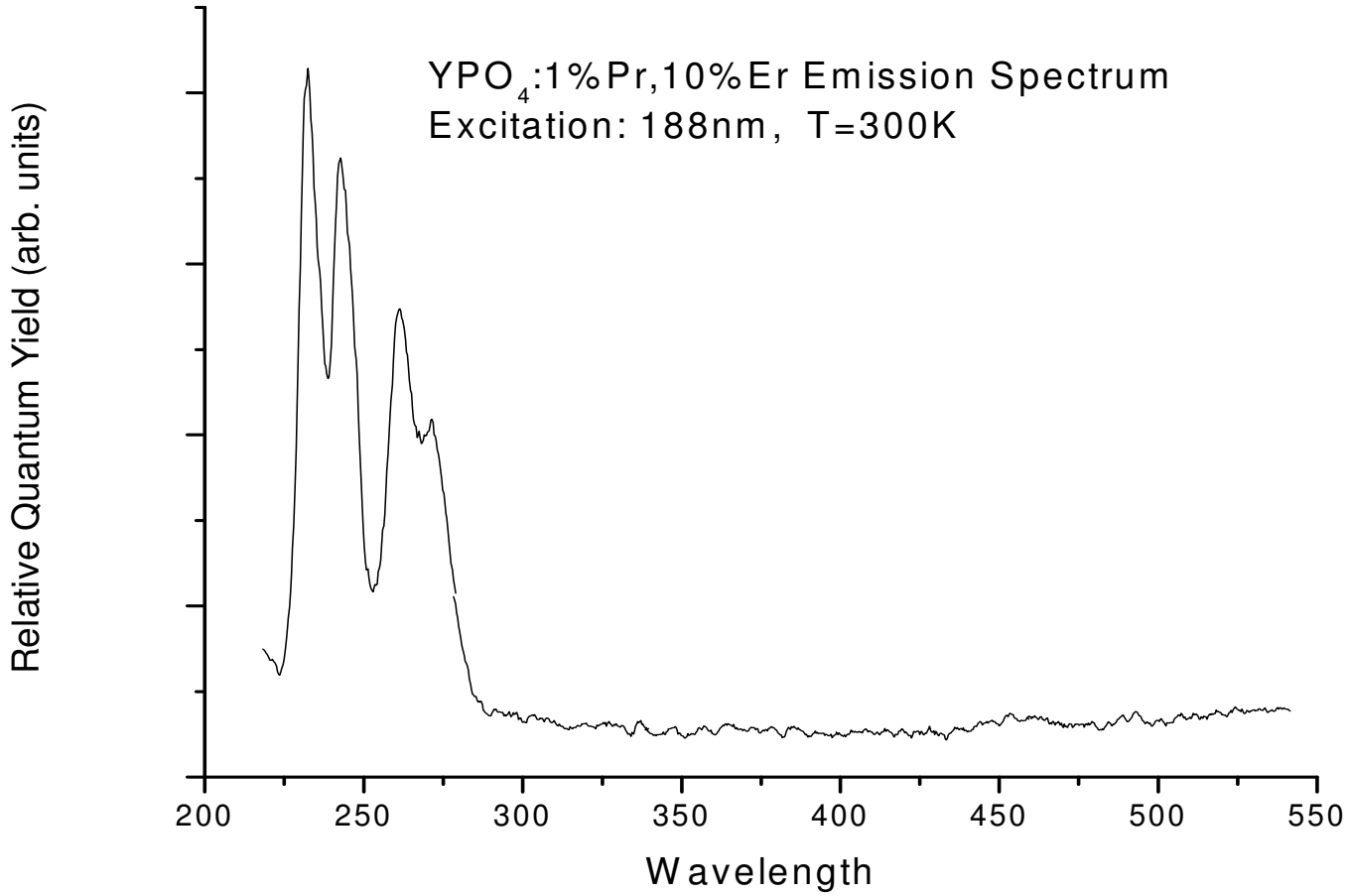
YPO4:1%Pr,10%Er Emission Spectrum
Excitation: 188nm, T=300K
Relative Quantum Yield (arb. units)
200
250
300
350
400
450
500
550
Wavelength

Fig. 4. 9

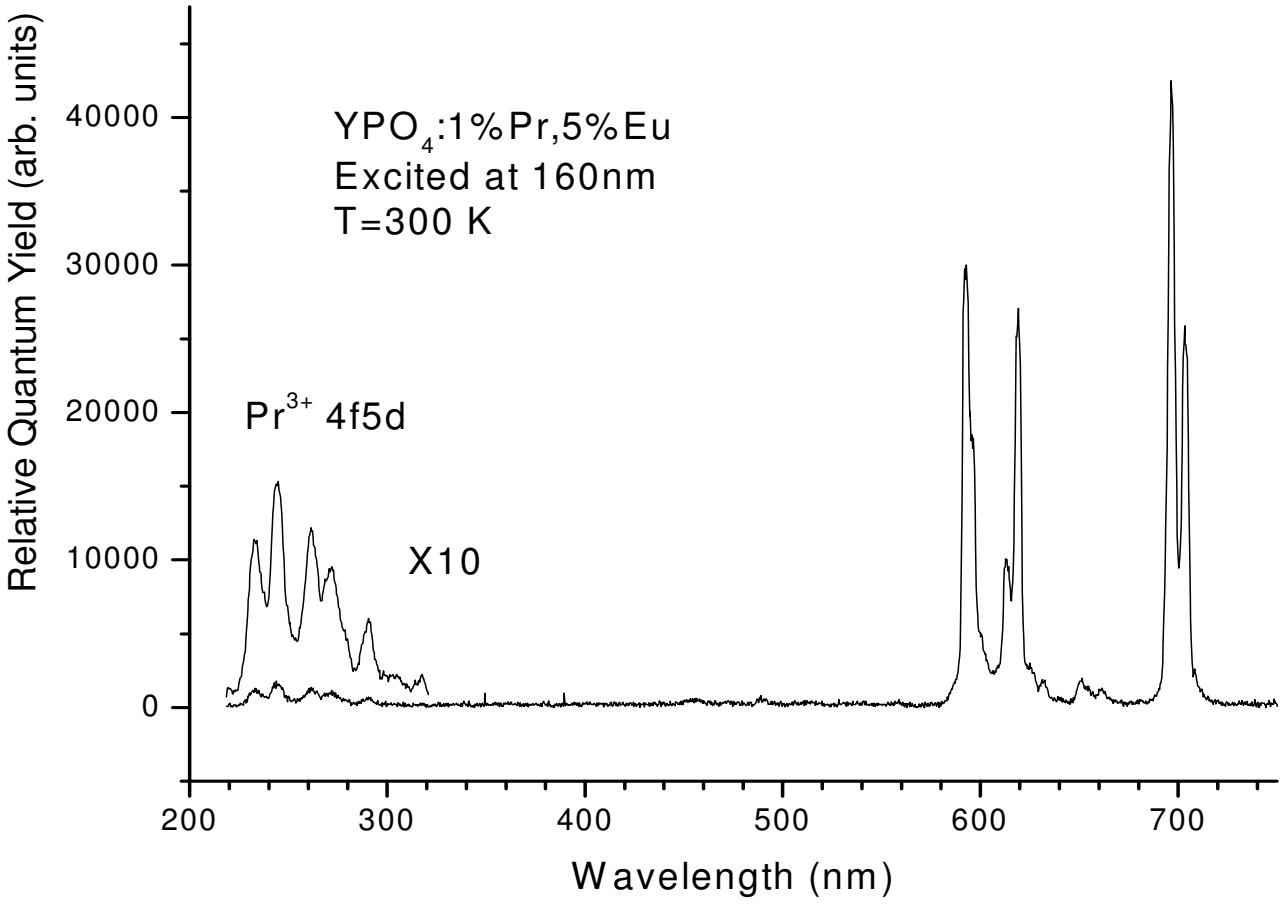
Relative Quantum Yield (arb. units)
40000
30000
20000
10000
0
YPO4:1%Pr,5%Eu
Excited at 160nm
T=300 K
Pr3+ 4f5d
X10
200
300
400
500
600
700
Wavelength (nm)

Fig. 4. 10

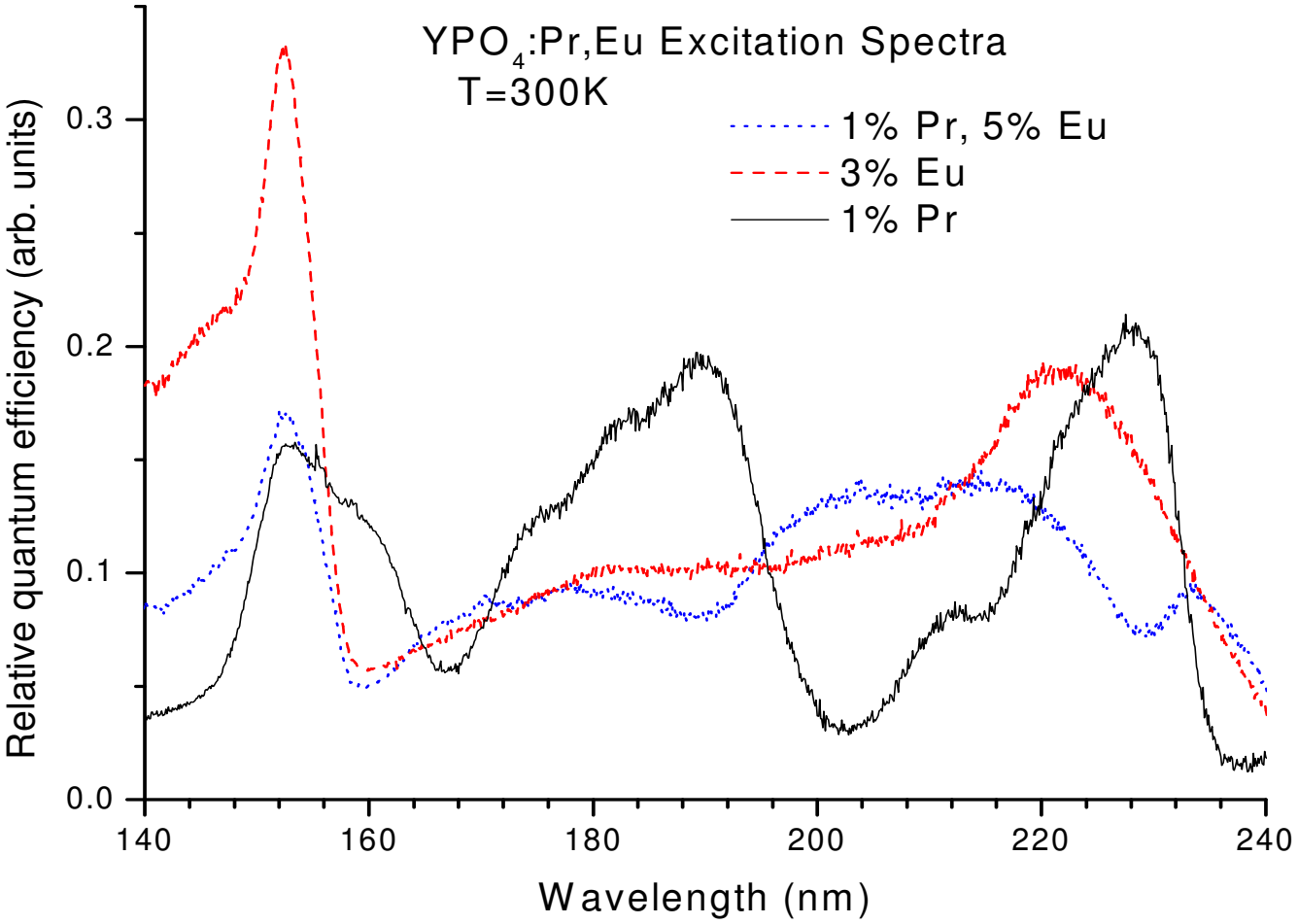
YPO4:Pr,Eu Excitation Spectra
T=300K
1% Pr, 5% Eu
3% Eu
1% Pr
Relative quantum efficiency (arb. units)
0.0
0.1
0.2
0.3
140
160
180
200
220
240
Wavelength (nm)

Fig. 4. 11

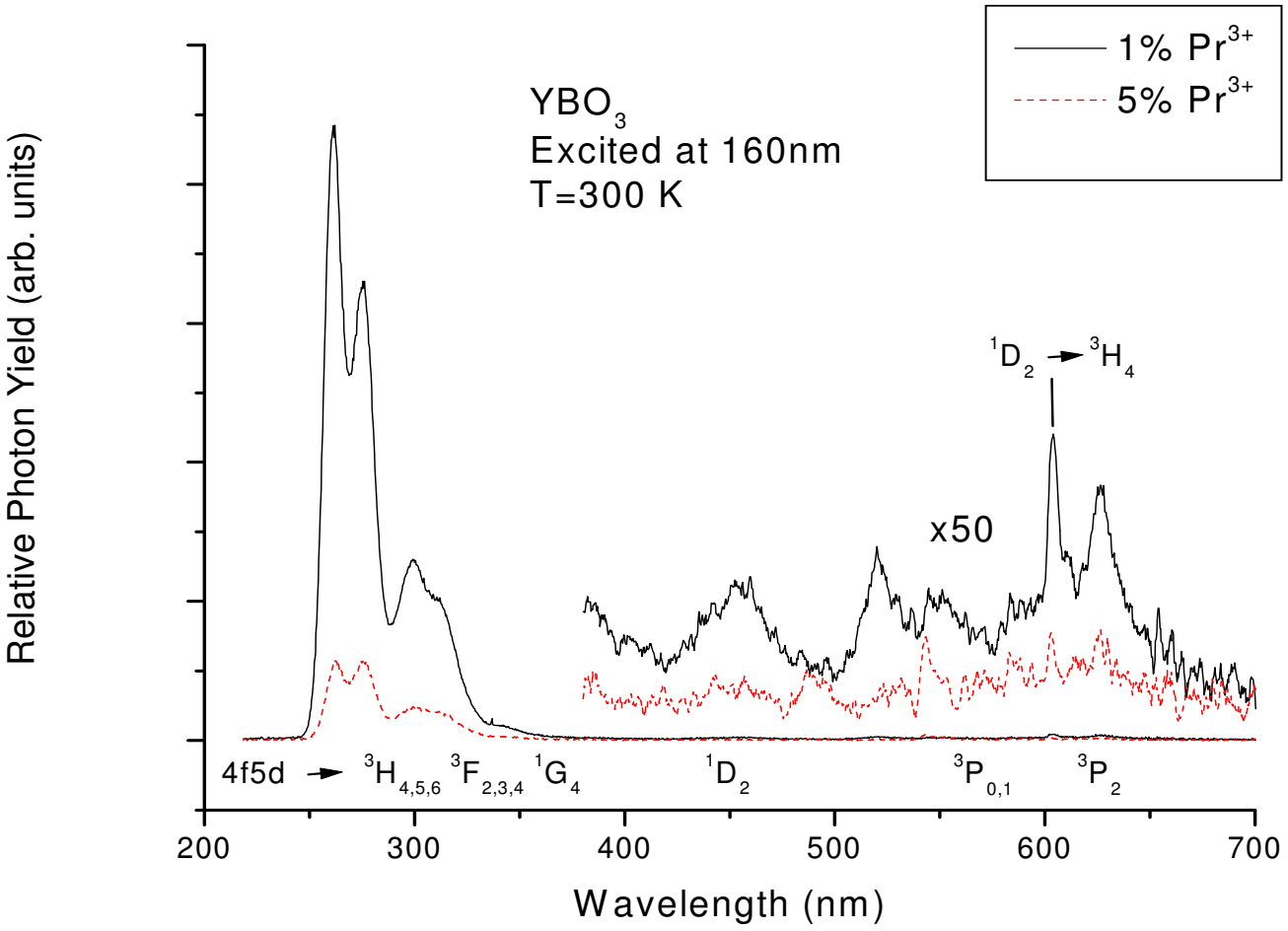
1% Pr3+
5% Pr3+
YBO3
Excited at 160nm
T=300 K
1D2 → 3H4
x50
4f5d → 3H4,5,6 3F2,3,4 1G4
1D2
3P0,1
3P2
Relative Photon Yield (arb. units)
Wavelength (nm)
200
300
400
500
600
700

Fig. 4. 12

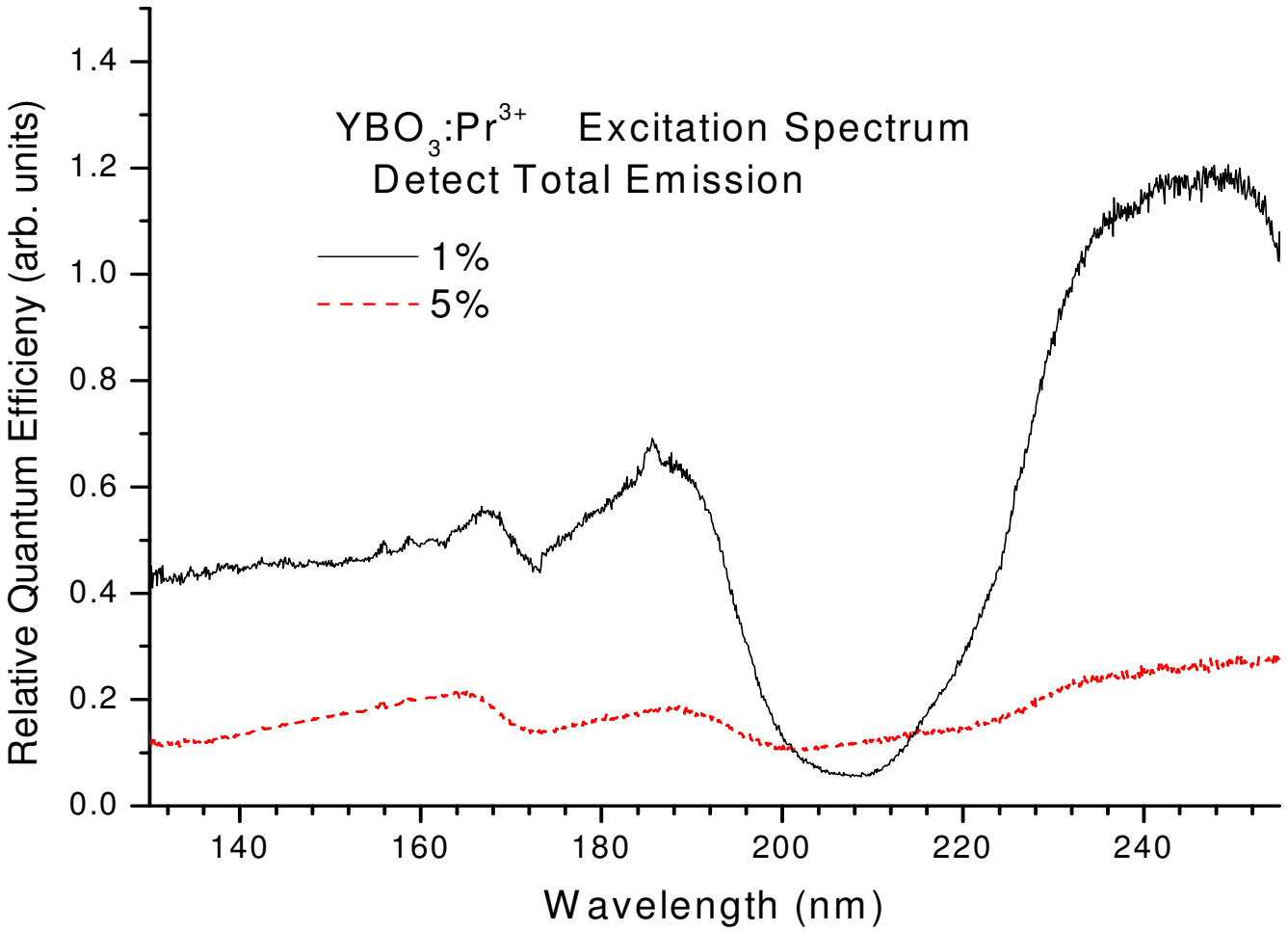
YBO3:Pr3+ Excitation Spectrum
Detect Total Emission
1%
5%
Relative Quantum Efficieny (arb. units)
Wavelength (nm)
0.0
0.2
0.4
0.6
0.8
1.0
1.2
1.4
140
160
180
200
220
240

Fig. 4. 13

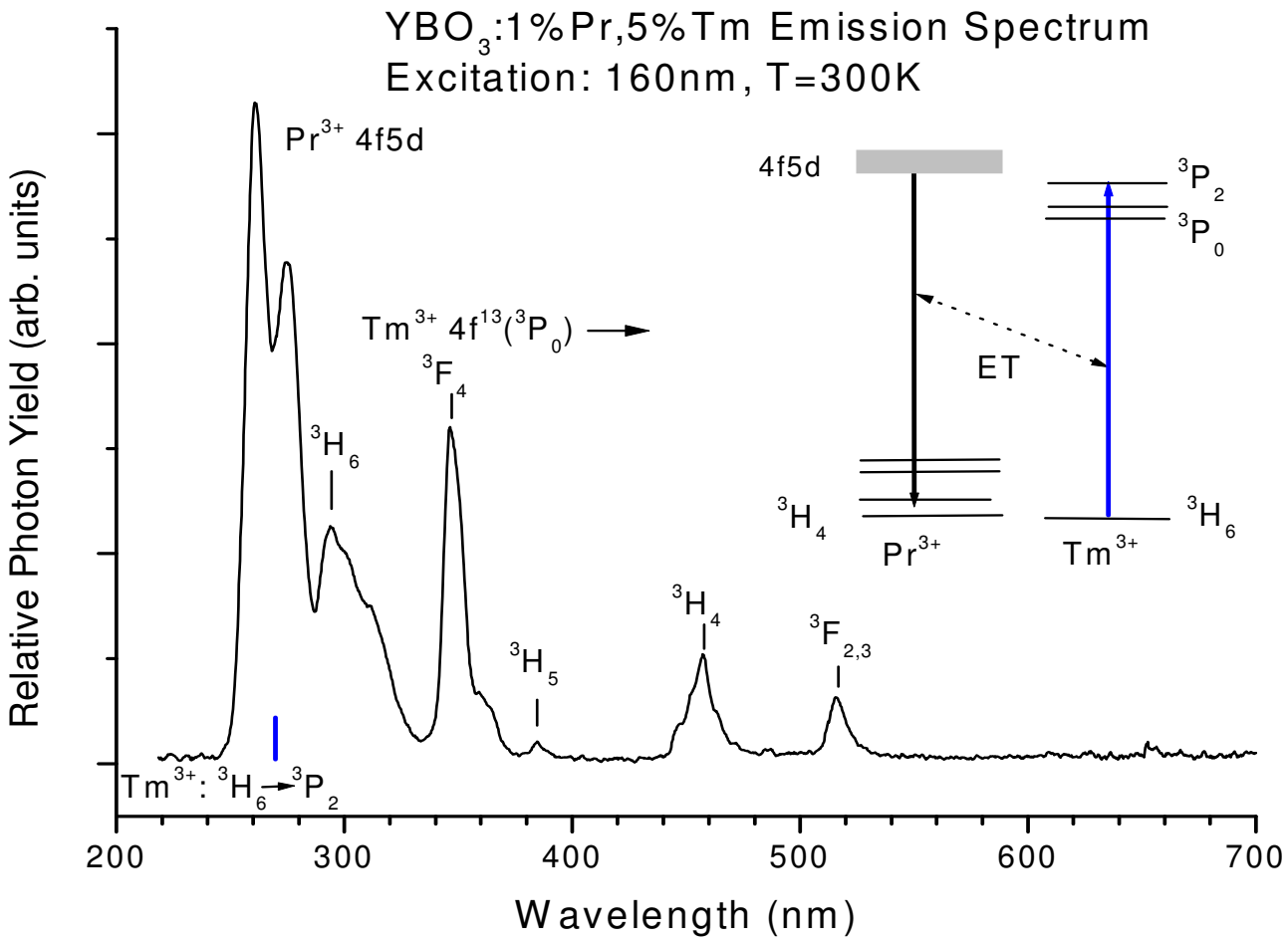
YBO3:1%Pr,5%Tm Emission Spectrum
Excitation: 160nm, T=300K
Pr3+ 4f5d
Tm3+ 4f13(3P0)
3F4
3H6
3H5
3H4
3F2,3
Tm3+: 3H6→3P2
4f5d
3P2
3P0
ET
3H4
3H6
Pr3+
Tm3+
Relative Photon Yield (arb. units)
200
300
400
500
600
700
Wavelength (nm)

Fig. 4. 14

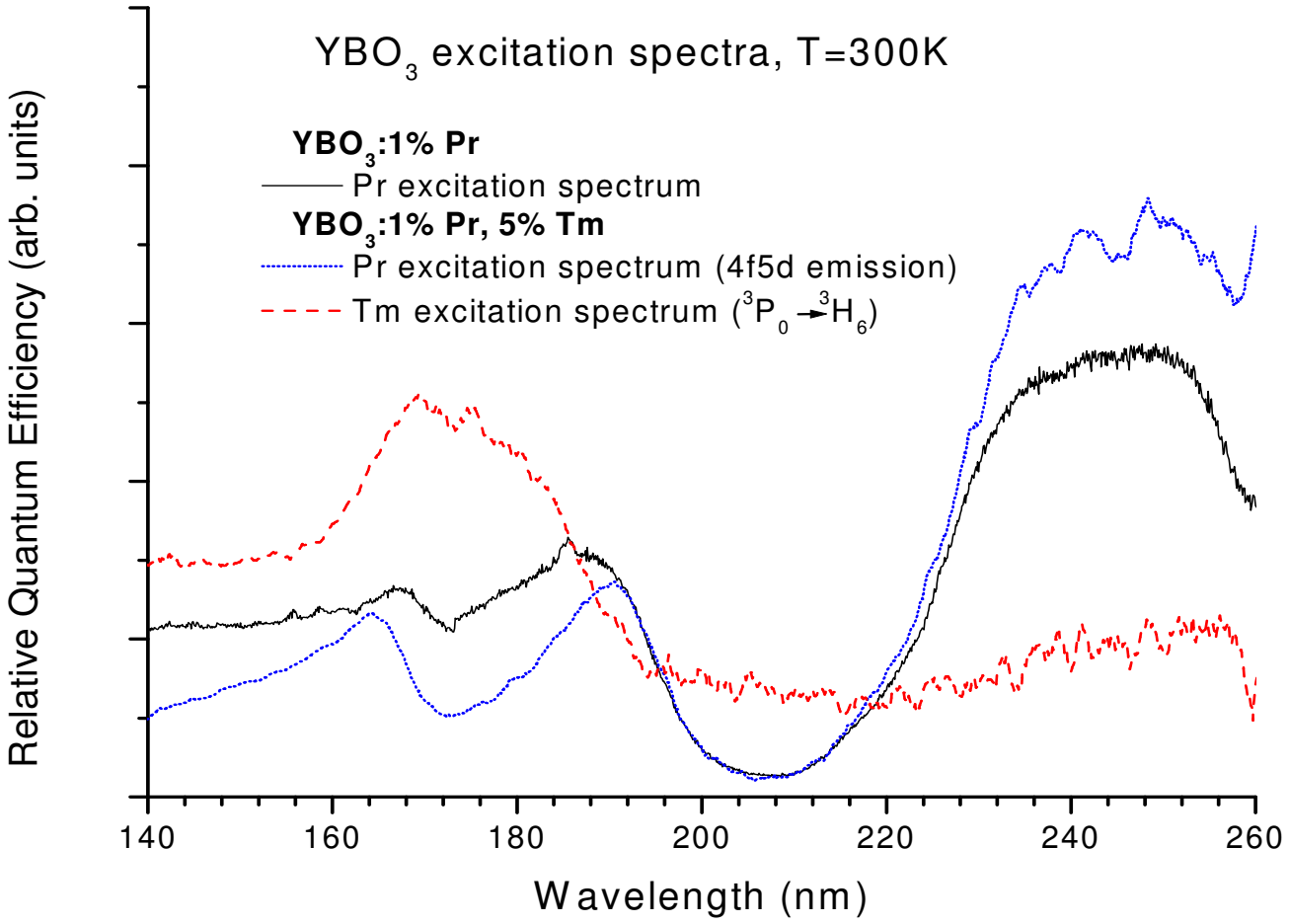
YBO3 excitation spectra, T=300K
YBO3:1% Pr
Pr excitation spectrum
YBO3:1% Pr, 5% Tm
Pr excitation spectrum (4f5d emission)
Tm excitation spectrum (3P0 → 3H6)
Relative Quantum Efficiency (arb. units)
140
160
180
200
220
240
260
Wavelength (nm)

Fig. 4.15

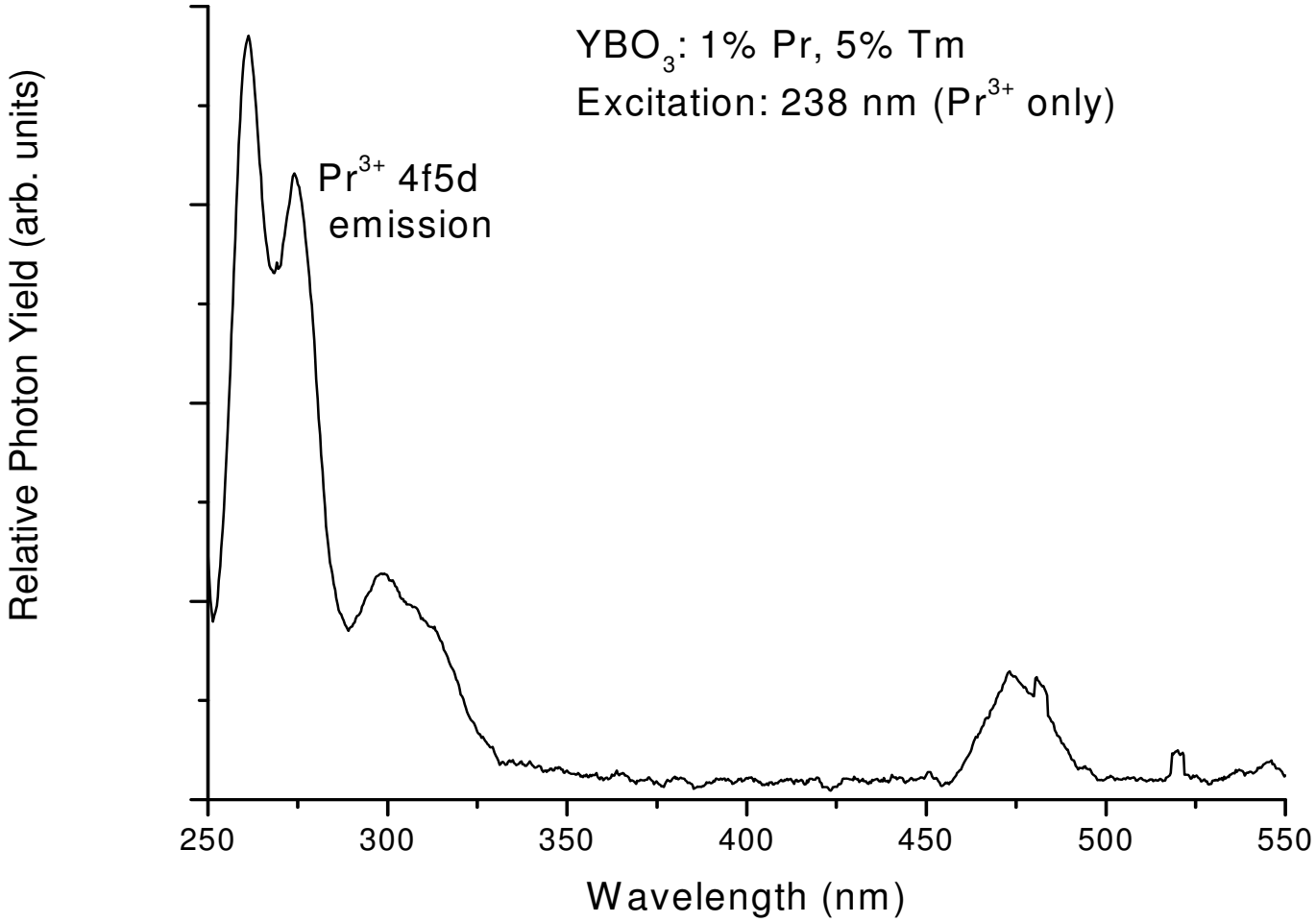
YBO3: 1% Pr, 5% Tm
Excitation: 238 nm (Pr3+ only)
Pr3+ 4f5d
emission
Relative Photon Yield (arb. units)
250
300
350
400
450
500
550
Wavelength (nm)

Fig. 4. 16

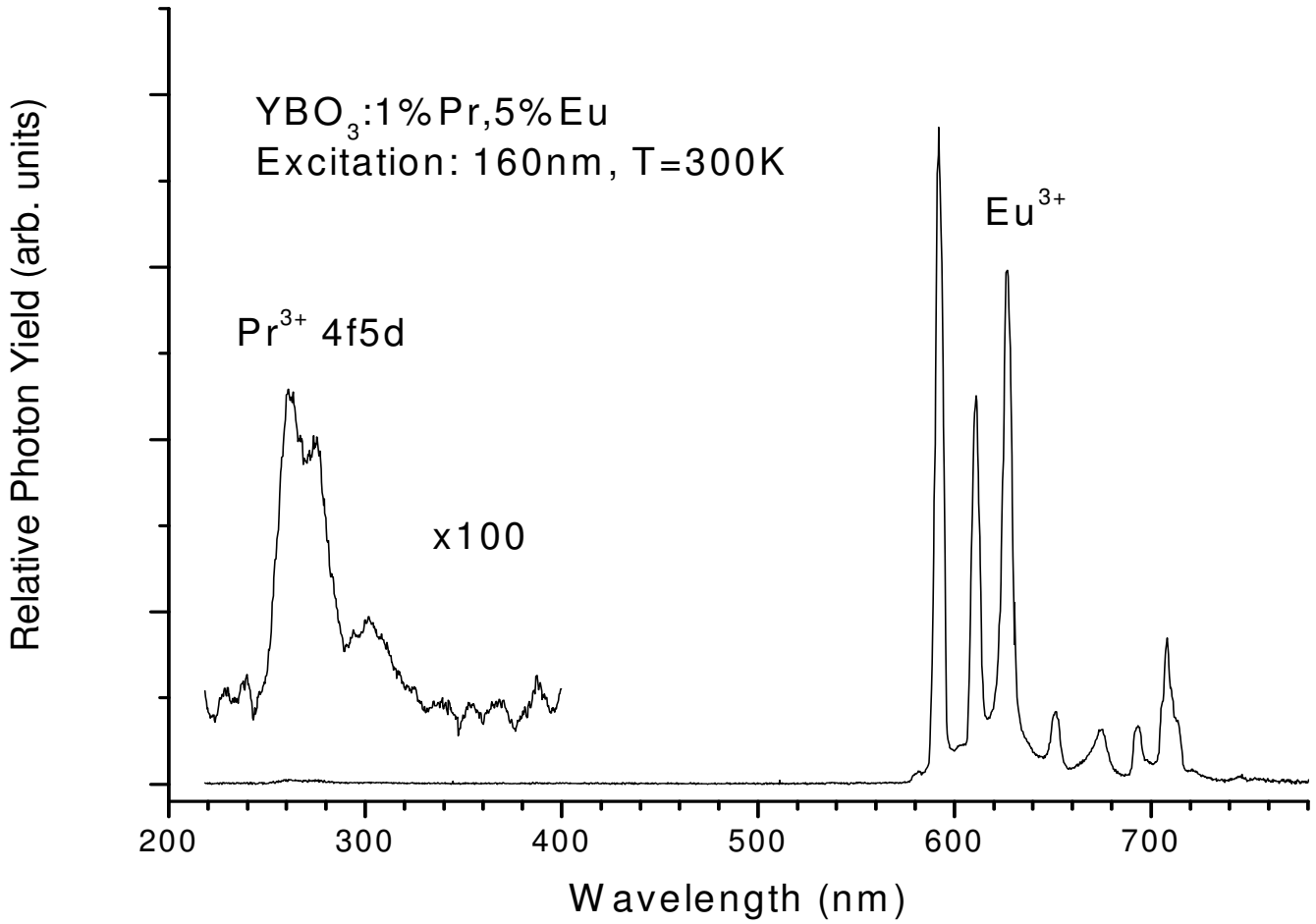
YBO3:1%Pr,5%Eu
Excitation: 160nm, T=300K
Pr3+ 4f5d
x100
Eu3+
Relative Photon Yield (arb. units)
200
300
400
500
600
700
Wavelength (nm)

Fig.4.17

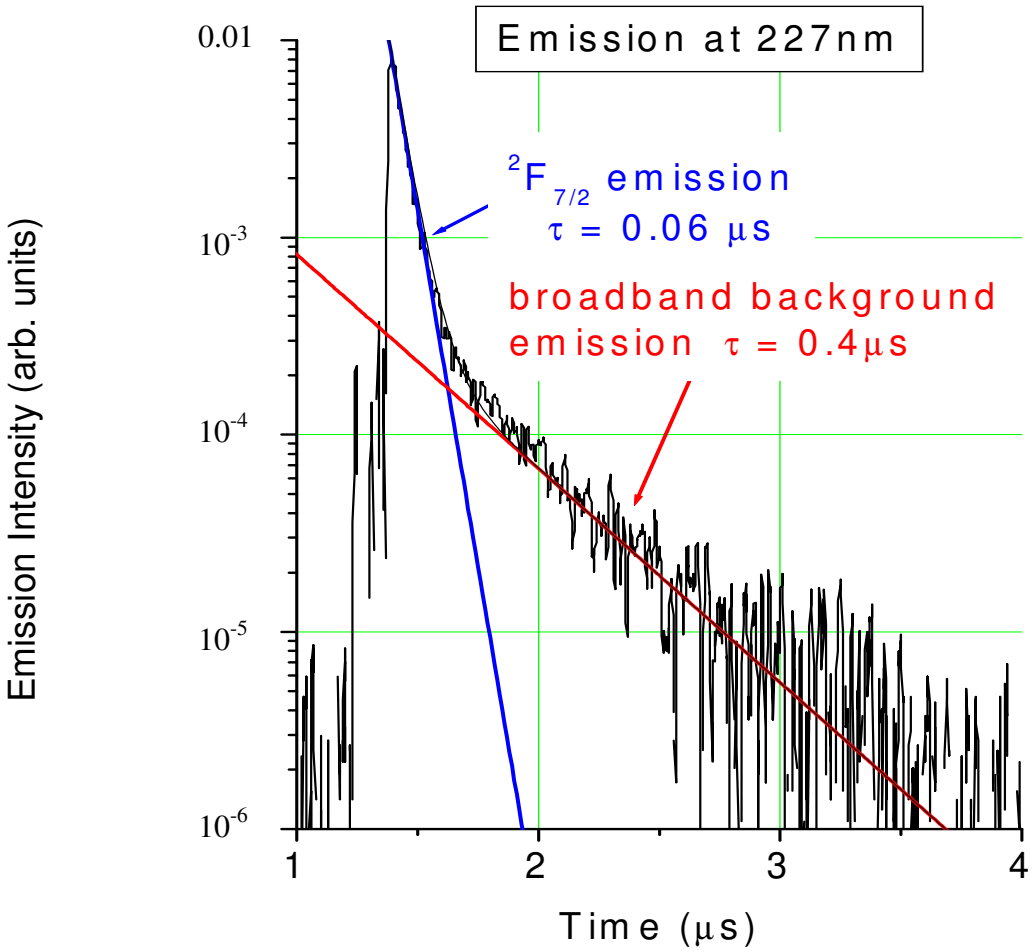
Emission at 227nm
$^2F_{7/2}$ emission
τ = 0.06 μs
broadband background
emission τ = 0.4μs
Emission Intensity (arb. units)
0.01
10^{-3}
10^{-4}
10^{-5}
10^{-6}
1
2
3
4
Time (μs)

Fig. 4.18

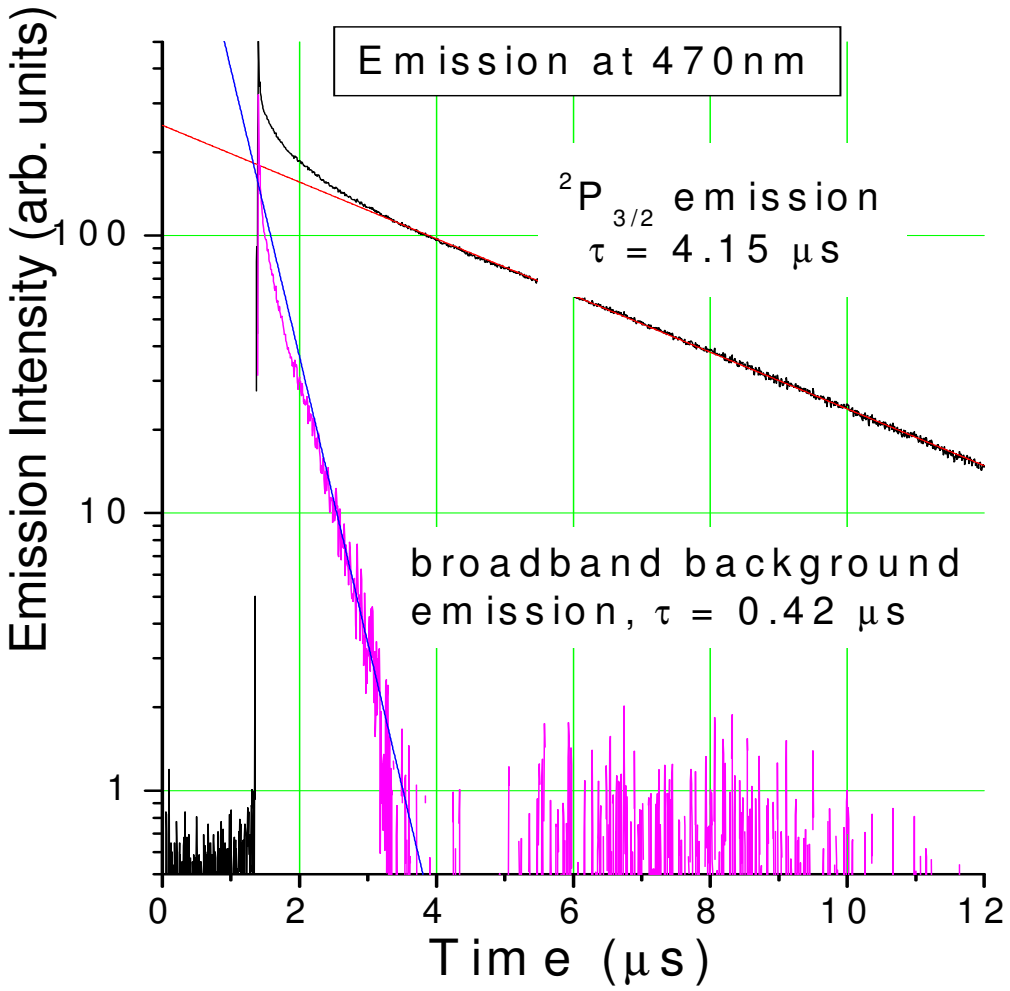
Emission at 470nm
$^2P_{3/2}$ emission
τ = 4.15 μs
broadband background
emission, τ = 0.42 μs
Emission Intensity (arb. units)
100
10
1
0
2
4
6
8
10
12
Time (μs)

Fig. 4.19

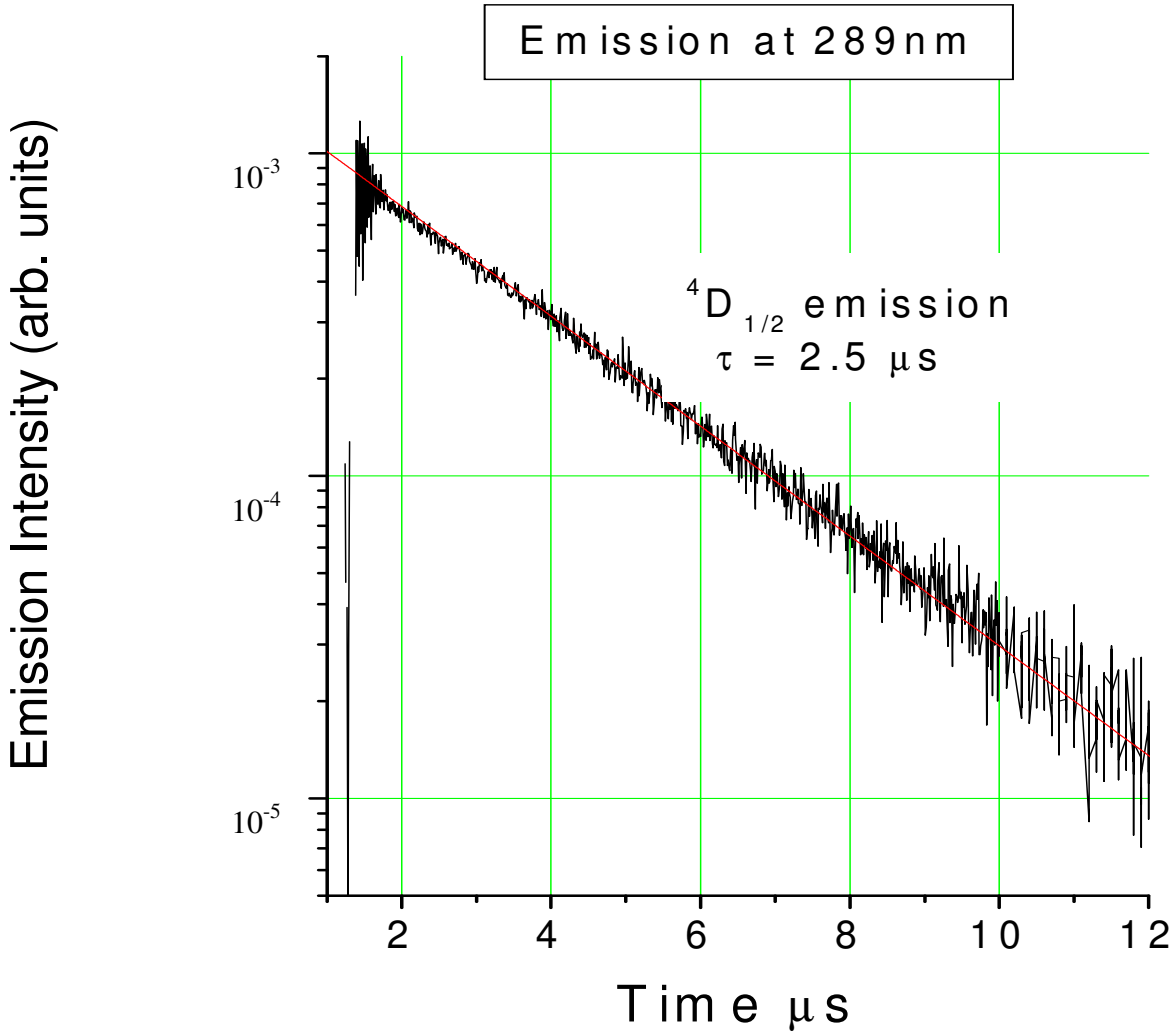
Emission at 289nm
$^4D_{1/2}$ emission
τ = 2.5 μs
Emission Intensity (arb. units)
10^{-3}
10^{-4}
10^{-5}
2
4
6
8
10
12
Time μs

Fig. 4.20

REFERENCES

[1] C. R. Ronda. J., Alloys Compounds 225, 534 (1995).

[2] A. M. srivastava and C. R. Ronda, the Electrochemical Society ***Interface*** Summer, 48 (2003).

[3] R.T. Wegh, H. Donker, K.D. Oskam, A Meijerink, J. Lumin. 82, 93 (1999).

[4] D. L. Dexter, Phys. Rev. 108 (3), 630 (1957).

[5] T. Justel, H. Nikol, and C. R. Ronda, *Angew. Chem. Int. Ed.,* 37, 3084 (1998).

[6] S. H. Lin, W. Z. Xiao and W. Dietz, Phys. Rev. E 47, 3698–3706 (1993).

[7] T. Kushida, J. Phys. Soc. Japan, 34, 1318 (1973).

[8] J. A. Caird, A. J. Ramponi and P. R. Staver, J. Opt. Soc. Am. B 8, 1391 (1991).

[9] R. T. Wegh, A Meijerink, Acta Phys. Polon. A 90, 333 (1996).

[10] K.D. Oskam, r.T. Wegh, H. Donker, E.V.D. van Loef, A. Meijerink, J. Alloys and Compds. 300/301, 421 (2000).

[11] R. T. Wegh, E. V. D. van Loef, A Meijerink, J. Lumin. 90, 111 (1999)

[12] K. Watanabe and Edward C. Y. Inn, J. Opt. Soc. Am. 43, 32 (1953)

[13] L. van Pieterson, M.F. Reid, G.W. Burdick, A. Meijerink, Phys. Rev.B 65, 045114 (2002).

[14] P. Dorenbos, J. Lumin. 91, 155 (2000).

APPENDIX A

The procedure for measuring emission spectra

1. Set VM502 to V configuration.
2. Set VM502 slit to 3mm.
3. Turn on the mechanical pump.
4. Turn on the turbo-pump, when the vacuum<100 milliTorr.
5. Open vacuum valve near the exit slit and open the main valve for VM502.
6. Turn on the deuterium lamp or the laser.
7. Turn on VM502 drive, move the wavelength position to 160nm or other value.
8. Set CCD slit to 400μm or other value.
9. Select optical filter for the CCD, if needed.
10. Define new folder for data.
11. Run CCD software in window.
12. Turn on the cooling system, and set temperature to -50°.
13. Define the file path.
14. Pay attention to the temperature of CCD. Do not accidentally switch off the cryostat.
15. Run the program to measure the emission spectra.

APPENDIX B

The procedure for measuring excitation spectra

1. Set VM502 VUV monochromator to **V** configuration
2. Set Slit S=400μm or other value.
3. Turn on the mechanical pump.
4. Turn on the turbo-pump when vacuum<100 milliTorr.
5. Open the vacuum valve near the exit slit and the valve for VM 502.
6. Select proper optical filter for PMT**.**
7. Set up PMT tube, carefully sealed from room light.
8. Turn on PMT power supply and set PMT high voltage to 900V or other value.
9. Turn on Kethley electrometer.
10. Write down the dark current of PMT.
11. Turn on the driver of VM502.
12. Turn on the deuterium lamp.
13. Define a folder in the data file address.
14. Run the software of VUV program.

    Select “excitaion”

    Define scan range in Anstrum

    Scan step: minimum 1 Anstrum.

Scan points: at each step, take some points for averaging. The average for spreadsheet file, the point data for raw file.

Experiment: put new file name

If you do not define new file name, the system asks for new file name after finishing the scan. However, the file in the spreadsheet does not contain the intensity data (all are zero), but the intensity data can be found in the raw files.

APPENDIX C

C. 1 Calibration of the PMT

We used a series of interference filters and the FEL Standard Lamp to calibrate the spectral response of the PMT. The intensity of emission is defined as

$$S = \lambda Q(\lambda) \int T(\lambda) I(\lambda) d\lambda$$

Here $Q(\lambda)$ is the quantum response of the PMT. $T(\lambda)$ is the transmission of the filter and $I(\lambda)$ is the output of the lamp. We put these filters before the lamp and measured the emission with the PMT. So we got

$$S_1 = \lambda_1 Q(\lambda_1) \int T_1(\lambda) I(\lambda) d\lambda$$

$$S_2 = \lambda_2 Q(\lambda_2) \int T_2(\lambda) I(\lambda) d\lambda$$

The spectral response is expressed as

$$P(\lambda) = \frac{Q(\lambda_2)}{Q(\lambda_1)} = \frac{\lambda_1}{\lambda_2} * \frac{S_2}{S_1} * \frac{\int T_1(\lambda) I(\lambda) d\lambda}{\int T_2(\lambda) I(\lambda) d\lambda}$$

C. 2 Correction of the excitation spectrum

(1) Correcting of the effect of scattered and background radiation

The Oriel 77341 PMT tube is sensitive to light in the spectral range 180 to 870 nm. Considering that UV beam is reflected from the window covering the sample, we should use optical filters to keep the light from going into the PMT. However, some optical filters emit in the visible under UV excitation. Its emission level will remain the same under identical

experimental conditions, while the emission intensity of samples themselves may vary from sample to sample. Therefore the interference of the filter emission can be recognized. To reduce the interference from the optics, smaller or larger incident angles other than 45° of the VUV beam to the sample surface can be used. As a result, the reflected VUV beam from the sample surface will not directly hit the optics so that the emission level from the optics will be reduced. Background light comes from the monochromator which filters the excitation source. The intensity slightly depends on wavelength, that is, the position of the grating. It is light at wavelengths other than that of the setting of the monochromator. This results from stray light that is scattered from non-smooth mirrors and zeroth or higher order diffractions of the grating. It is difficult to remove the background light since the traveling direction of the background light is similar to the pumping light. It can be reduced by using smaller or larger incident angles than 45^{o} of the pump beam in order to reduce the background interference.

(2) Correcting for the presence of multiple emission wavelengths where the quantum efficiency of the PMT has different values

We used the correction factor weighted average of $P(\lambda)\ T(\lambda)$ weighted by the emission spectrum of the sample and of the sodium salicylate.

$$C_{sample} = \frac{\int E_{sample}(\lambda)d\lambda}{\int E_{ref}(\lambda)d\lambda} * \frac{\int E_{ref}(\lambda)T(\lambda)P(\lambda)d\lambda}{\int E_{sample}(\lambda)T(\lambda)P(\lambda)d\lambda}$$

Here $E(\lambda)$ is the emission spectrum obtained by the CCD.

(3) For the consequence of the emission spectrum changing as a function of excitation wavelength, we assume the emission spectrum is independent of the excitation wavelength.

APPENDIX D

The procedure for measuring decay time

1. Turn on the oscilloscope.
2. Rename the file.
3. Select the format of the file which will be saved.
4. Select proper optical filter for PMT**.**
5. Set up PMT tube, carefully sealed from room light.
6. Turn on PMT power supply and set PMT high voltage to 900V or other value
7. Turn on the mechanical pump.
8. Turn on the turbo-pump when vacuum<100 milliTorr.
9. Turn on the laser.